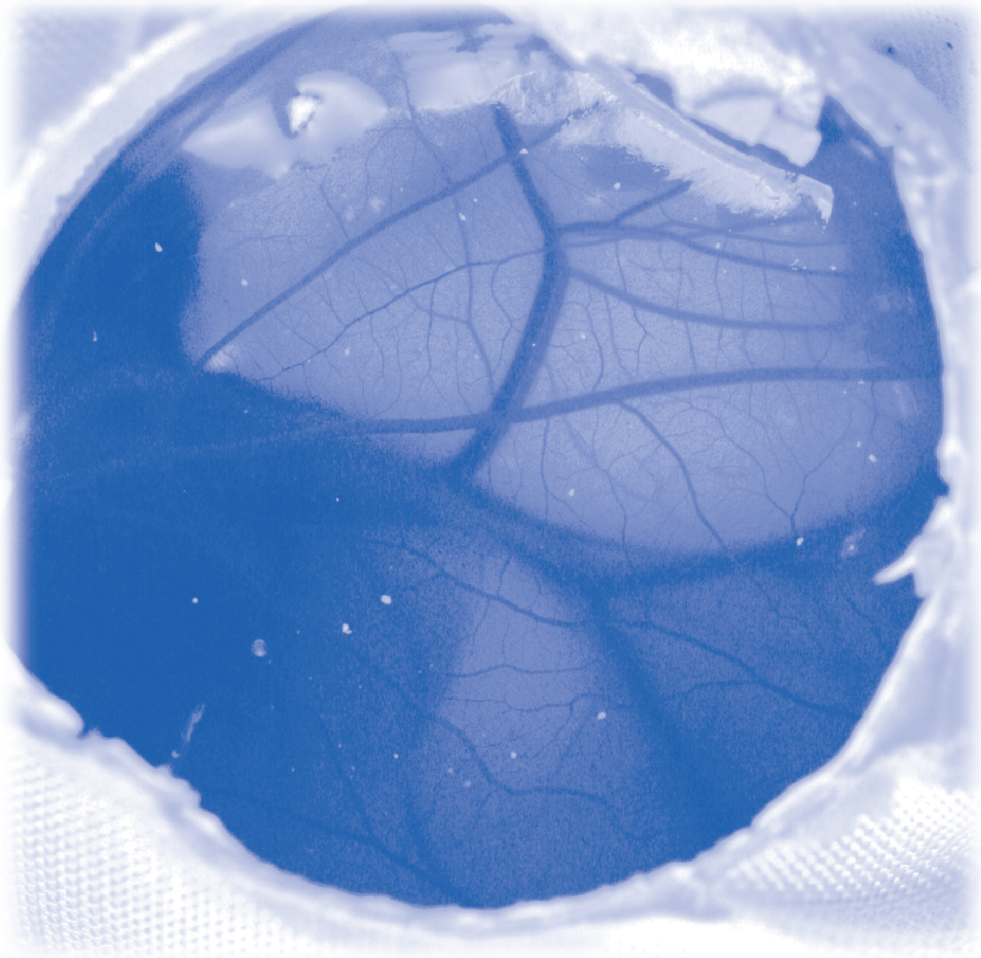




STUDIA UNIVERSITATIS
BABEȘ-BOLYAI



BIOLOGIA

2/2011

YEAR
MONTH
ISSUE

(LVI) 2011
DECEMBER
2

S T U D I A
UNIVERSITATIS BABEȘ-BOLYAI
BIOLOGIA

2

Desktop Editing Office: 51ST B.P. Hasdeu, Cluj-Napoca, Romania, Phone + 40 264-40.53.52

SUMAR – CONTENTS – SOMMAIRE – INHALT

R. MICLEA, C. E. PUIA, A Phenotypical Characterization of <i>Botrytis cinerea</i> Pers. Strains Isolated from Ornamental Plants	3
V. BERCEA, C. COMAN, C. SICORA, N. DRAGOȘ, The Photochemical PS II Activity in Cyanobacterial Strains Belonging to the Nostocales Group in Anaerobiosis Conditions.....	13
V. BERCEA, A. BICA, B. DRUGĂ, C. SICORA, N. DRAGOȘ, The Effect of Argon-induced Anaerobiosis on the Activity of Photosystem PS II in Some Nostocales Species.....	27
M. MOHAMADHASANI, M. HAVESHKI, A Mathematical Modeling for an Epidemic with Respect to the Immigration	39
R. M. MAXIM, M.-C. ALUPEI, S. TRIPON, M. BANCIU, Evaluation of the Inhibitory Effects of Statins on Blood Vessel Development - Prospects for Antiangiogenic Therapy of Cancer	49

E. LICĂRETE, C. SITARU, M. T. CHIRIAC, Myeloperoxidase but not Superoxide Dismutase Has a Protective Effect in the <i>Ex Vivo</i> Model of Bullous Pemphigoid.....	59
C. V. SIMULE, M. DRĂGAN BULARDA, Effects of Zinc, Lead and Cadmium Pollution on the Structure and Activities of Soil Bacterial Community	71

All authors are responsible for submitting manuscripts in comprehensible US or UK English and ensuring scientific accuracy.

Original picture on front cover: *Chorioallantoic membrane (CAM) of the chick embryo*

© Manuela Banciu.

==SHORT COMMUNICATION==

PHENOTYPICAL CHARACTERIZATION OF *BOTRYTIS CINEREA*
PERS. STRAINS ISOLATED FROM ORNAMENTAL PLANTS

RALUCA MICLEA^{1,✉} and CARMEN EMILIA PUIA¹

SUMMARY. The pathogenic fungus *Botrytis cinerea* Pers., found throughout the world, attacks over 250 species of plants. *Botrytis cinerea* Pers. is responsible for the gray rot of grapes and other fruits and vegetables that can strongly affect crop quality and quantity. The attack occurs on all aerial organs of the plants: stems, leaves, peduncles especially on flowers. Infected tissues are covered by a grayish-white coating, consisting of mycelium and sporulation. Following the attack, tissues soften, become brown in color and dry. The aim of this study was to determine the differences between the dimensions of conidia, number and distribution of sclerotia for several isolates cultivated on two different culture media, Potato Dextrose Agar (PDA) and Czapek. In this experiment, the length and width of 100 conidia from each *Botrytis cinerea* Pers. isolate were measured. The isolates were obtained from 9 species of ornamental plants: *Cyclamen* sp., *Dahlia* sp., *Rosa* sp., *Petunia* sp., *Geranium* sp., *Taxus* sp., *Chrysanthemum* sp., *Hybiscus* sp., and *Fuchsia* sp.

Keywords: *Botrytis*, conidia, fungus, disease, rot.

Introduction

Botrytis cinerea Pers.:Fr., the anamorph of *Botryotinia fuckeliana* Whetzel causes grey mould on a high number of crop plants worldwide in the temperate zones (Vaczy *et al.*, 2010). It is most destructive on mature or senescent tissues of dicotyledonous hosts but it usually gains entry to such tissues at an earlier stage in crop development and remains quiescent for a considerable period before rapidly rotting tissues when the environment is conducive and the host physiology changes (Williamson *et al.*, 2007). Therefore, serious damage is caused following harvest of apparently healthy crops and the subsequent transport to distant markets where the losses become evident (Elad *et al.*, 2004).

Droby and Lichter (2004) provide a comprehensive list of postharvest rots caused by *Botrytis cinerea* Pers.; these range from grey mould on different plant organs, including flowers, fruits, leaves, shoots and soil storage organs.

^{1, ✉} **Corresponding author:** Faculty of Agricultural Sciences, University of Agricultural Sciences and Veterinary Medicine, 3-5 Mănăştur Str., Cluj-Napoca, Romania. E-mail: ralu_bio@yahoo.com

Botrytis cinerea Pers. causes blossom blight, bud rot, stem canker, stem and crown rot, cutting rot, leaf blight and damping-off or seedling blight. Blossom blight and bud blight appears on ornamentals such as asters, azalea, begonia, carnation, chrysanthemum, cyclamen, dahlia, geranium, marigold, peony, petunia, roses etc. (<http://web.aces.uiuc.edu>).

Botrytis cinerea Pers. was chosen for four main reasons: it is a facultative pathogen that can be grown on culture media in the laboratory; isolates are abundant on a wide variety of host plants; a perfect state has been recorded which, even though it is rare, means that it is feasible to derive sexual progeny; it is economically important, causing losses in fruit and vegetable crops (Grindle, 1979).

The common conidial state, *Botrytis cinerea* Pers., consists of mycelia that give rise to asexual spores and sclerotia (tough, black, irregular-shaped aggregations of hyphae). Sclerotia can withstand harsh environmental conditions, and the fungus probably overwinters in this form to provide fresh colonies and spores in spring (Grindle, 1979).

Features such as sclerotial size, form and conidium size are useful in delimiting some species, but many species are morphologically similar and growing conditions significantly influence variation (Beever and Weeds, 2004).

In our study we have isolated *Botrytis cinerea* Pers. fungus from 9 species of ornamental plants: *Cyclamen* sp., *Dahlia* sp., *Rosa* sp., *Petunia* sp., *Geranium* sp., *Taxus* sp., *Chrysanthemum* sp., *Hybiscus* sp., and *Fuchsia* sp. we've grown it on two culture media PDA and Czapek, in Petri plates.

The purpose of the research was to observe cultural features such as: the colony diameter, the conidia and the sclerotia development, the size and the shape of the conidia and the number and the distribution of the sclerotia in order to establish if there are any phenotypical differences between the isolates of this pathogen on the two culture media.

Materials and methods

In our experiments, the *Botrytis cinerea* Pers. strains were isolated on two different media (Potato Dextrose agar - PDA and Czapek agar), using 8cm Petri plates.

The *Botrytis cinerea* Pers. colonies were analyzed for *in vitro* features of the strains: the growth of the colony and the morphological characteristics of the fungus.

The media were prepared according to Constantinescu's (1974) recipe (Czapek: 3 g Na NO₃, 1g K₂ HPO₄, 0.5 g Mg SO₄ x 7 H₂O, 0.5 g KCl, 0.01 g FeSO₄ x 7H₂O, 30 g sucrose, 15 g agar, 1000 ml distilled water and PDA: 200 g potato, 20 g dextrose, 20 g agar, 1000 ml distilled water).

Given the literature data, the fungal inoculation was initiated in the central point of the plate with plugs of mycelium (5 mm in diameter) followed by incubation at 25°C.

The length and width of 100 conidia from each isolate were measured at 40x magnification with the program Motic Images.

The diameter of the colonies was measured daily until the colony occupied the entire plate.

The appearance of the fructifications and the sclerotia formation were examined at 3, 6, 9, 12 days and 20 days after the inoculation. We examined the color, the shape and the distribution of the sclerotia.

Results and discussions

The *Botrytis cinerea* Pers. colonies developed on PDA medium were measured for 5 days, the majority reaching the maximum development in the 4th day (Table 1).

Table 1.

The colony diameter for *Botrytis cinerea*
Pers. isolated on PDA medium

No	Isolate	Colony diameter (cm) on PDA				
		Day1	Day2	Day3	Day4	Day5
1	<i>Rosa</i> sp.	0.2	2.93	4.86	7.86	8
2	<i>Hybiscus</i> sp.	0.6	2.7	6	8	8
3	<i>Fuchsia</i> sp.	0.5	3	5.3	8	8
4	<i>Chrysanthemum</i> sp.	0.6	3.3	6.3	8	8
5	<i>Geranium</i> sp.	0.83	3.56	5.63	8	8
6	<i>Dahlia</i> sp.	0.2	2.76	4.63	7.6	8
7	<i>Cyclamen</i> sp.	0.63	2.63	4.26	6.6	8
8	<i>Petunia</i> sp.	0.53	3.6	5.73	8	8
9	<i>Taxus</i> sp.	0.2	3.23	5.36	8	8

The isolates from cyclamen, dahlia and rose did not occupy all the Petri plates, the colonies having 6.6, 7.6 respectively 7.86 cm in diameter, on the 4th day.

Concerning the growth of the colonies on the Czapek medium we can assert that the fungus had a slow development, no colony reached 8 cm in diameter on the fourth day, compared to the colonies on PDA. All the colonies reached the maximum development only on the seventh day (Table 2.)

Table 2.

**The colony diameter for *Botrytis cinerea*
Pers. isolated on Czapek medium**

No	Isolate	Colony diameter (cm) on Czapek						
		Day1	Day2	Day3	Day4	Day5	Day6	Day7
1	<i>Rosa</i> sp.	0.73	1.93	3.5	4.8	7.33	8	8
2	<i>Hybiscus</i> sp.	0.63	3.2	5.16	7.16	8	8	8
3	<i>Fuchsia</i> sp.	0.5	0.93	1.86	6.36	7.8	8	8
4	<i>Chrysanthemum</i> sp.	0.3	1.43	2.53	6.24	7.20	8	8
5	<i>Geranium</i> sp.	0.63	2.06	4.1	6.16	7.83	8	8
6	<i>Dahlia</i> sp.	0.46	0.83	1.83	6.63	7.36	7.63	8
7	<i>Cyclamen</i> sp.	0.4	2.2	4.73	6.86	8	8	8
8	<i>Petunia</i> sp.	0.4	0.63	1.43	6.1	6.06	6.5	8
9	<i>Taxus</i> sp.	0.56	1.93	4.03	5.7	8	8	8

Table 3.

**The occurrence of the sporulation and sclerotia
for PDA and Czapek culture media**

Isolate	PDA				CZAPEK			
	Day3	Day6	Day 9	Day 12	Day 3	Day 6	Day 9	Day 12
<i>Rosa</i> sp.	Sp- Sc-	Sp+ Sc-	Sp+++ Sc+	Sp++++ Sc+	Sp- Sc-	Sp- Sc-	Sp- Sc-	Sp- Sc-
<i>Hybiscus</i> sp.	Sp-Sc-	Sp-Sc-	Sp++ Sc	Sp++ Sc+	Sp- Sc-	Sp- Sc-	Sp- Sc-	Sp- Sc-
<i>Fuchsia</i> sp.	Sp-Sc-	Sp++ Sc-	Sp+++ Sc	Sp+++ Sc-	Sp- Sc-	Sp++ Sc-	Sp+++ Sc-	Sp++++ Sc+
<i>Chrysanthemum</i> sp.	Sp-Sc-	Sp+ Sc-	Sp++ Sc-	Sp++ Sc-	Sp- Sc-	Sp- Sc-	Sp- Sc-	Sp- Sc-
<i>Geranium</i> sp.	Sp-Sc-	Sp-Sc-	Sp+++ Sc+	Sp++++ Sc+++	Sp- Sc-	Sp- Sc-	Sp- Sc-	Sp- Sc-
<i>Dahlia</i> sp.	Sp-Sc-	Sp-Sc-	Sp+ Sc	Sp+ Sc+	Sp- Sc-	Sp- Sc-	Sp+ Sc-	Sp++ Sc++
<i>Cyclamen</i> sp.	Sp-Sc-	Sp+ Sc-	Sp++ Sc+	Sp+++ Sc++	Sp- Sc-	Sp- Sc-	Sp- Sc-	Sp- Sc-
<i>Petunia</i> sp.	Sp+ Sc-	Sp++S c++	Sp+++ Sc+++	Sp+++ Sc++++	Sp- Sc-	Sp- Sc-	Sp- Sc-	Sp- Sc-
<i>Taxus</i> sp.	Sp-Sc-	Sp-Sc-	Sp- Sc++++	Sp- Sc++++	Sp- Sc-	Sp- Sc-	Sp- Sc-	Sp- Sc-

Sporulation: - no spores, + low, ++ good, +++ medium, ++++ very good

Sclerotia : + (0-20), ++ (20-40), +++ (40-60), ++++ (> 60)

Studying the cultural characters of *Botrytis cinerea* Pers. colonies grown on two different culture media we can affirm that the fungus had a better growth rate on PDA medium. On the Czapek medium only 2 isolates formed sclerotia and sporulated (*Fuchsia* sp., *Dahlia* sp.) the most abundant sporulation was observed on the *Fuchsia* sp. isolate (Table 3).

The mycelium was branched, septate, hyaline to brown. Conidiophores were observed arising directly from the mycelium or from the germinated sclerotia. They were more or less straight, septate, monopodial branched towards the apex (Fig. 1).

Different growth patterns were observed on PDA medium, at room temperature, under light. They were compact radial or in concentric rings, cottony, warty or powdery. The colonies were white, dirty white, grayish white (Fig. 2) or hyaline at first, becoming light gray, dark gray.



Fig. 1. *Botrytis cinerea* Pers. sporulation – conidiophores and conidia



Fig. 2. *Botrytis cinerea* Pers. colony grown on PDA medium after 12 days, showing mycelium and sclerotia

The conidia were solitary, hyaline or pale brown but in mass they seemed gray becoming darker with age. The forms of the conidia observed in the microscopic fields were ellipsoidal or sometimes globose. They were smooth, often with a slightly protuberant hilum and unicellular (Fig. 3).

To study the conidial morphology we have microscopically analyzed 100 conidia for each isolate; the length and width of the conidia were measured using Motic Images program, at 40x magnification (Fig. 3).

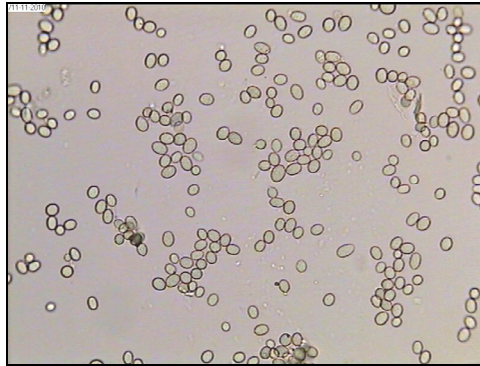


Fig. 3. Microscopical view of *Botrytis cinerea* Pers. conidia

The length of the conidia on PDA medium took values between 9.37 μm on *Hibiscus* sp. isolate, followed by *Taxus* sp. isolate with 9.38 μm and 12.04 μm in *Fuchsia* sp. isolate. The width had the lowest values in *Taxus* sp. conidia (7.94 μm) and the highest in the case of *Fuchsia* sp. isolate (10.2 μm) (Table 4).

Table 4.

The average length/width of conidia (μm) from *Botrytis cinerea* Pers. isolates on PDA and Czapek culture media

No	Isolate	PDA	CZAPEK
1.	<i>Rosa</i> sp.	10.32/8.81	-
2.	<i>Hibiscus</i> sp.	9.37/8.29	-
3.	<i>Fuchsia</i> sp.	12.04/10.2	11.4/9.7
4.	<i>Chrysanthemum</i> sp.	10.96/8.45	-
5.	<i>Geranium</i> sp.	11.27/9.42	-
6.	<i>Dahlia</i> sp.	10.79/8.89	10.9/9.5
7.	<i>Cyclamen</i> sp.	11.64/9.3	-
8.	<i>Petunia</i> sp.	11.9/8.86	-
9.	<i>Taxus</i> sp.	9.38/7.94	-

Only 2 of the isolates cultivated on the Czapek medium sporulated and the length values were 11.4 μm for the *Fuchsia* sp. isolate and 10.9 for the *Dahlia* sp. isolate. The width of the spores was 9.5 μm in *Dahlia* sp. and 9.7 μm in *Fuchsia* sp. isolate (Table 4).

All the species of *Botrytis* genus form sclerotia but differences in size and shape can be observed, according to every isolate and cultural conditions. As we can observe, in Table 5 all the isolates grown on PDA medium formed sclerotia but for the isolates grown on Czapek medium only in two cases the resistant bodies were formed (Table 5).

Table 5.

The number of sclerotia formed on PDA and Czapek media

No	Isolate	PDA	Czapek
1.	<i>Rosa</i> sp.	71	-
2.	<i>Hybiscus</i> sp.	34	-
3.	<i>Fuchsia</i> sp.	200	12
4.	<i>Chrysanthemum</i> sp.	126	-
5.	<i>Geranium</i> sp.	155	-
6.	<i>Dahlia</i> sp.	57	28
7.	<i>Cyclamen</i> sp.	15	-
8.	<i>Petunia</i> sp.	232	-
9.	<i>Taxus</i> sp.	58	-

The number of the sclerotia formed on the plates with PDA medium (Fig. 4) had the highest value (232 sclerotia) on the plate with the *Petunia* sp. isolate and the lowest number was formed by the cyclamen isolate (15). On Czapek medium only *Fuchsia* sp. and *Dahlia* sp. isolates formed 12, respectively 28 sclerotia (Table 5).

In some isolates sclerotia were abundant, but rare or absent in others. The resistant bodies were often superficial or deeply imbedded in the agar and adherent to the bottom of the Petri plate.

The distribution models of the sclerotia isolates were produced on concentric rings, along the edges of the Petri dish or scattered irregularly (Fig. 4). They were firmly attached to the surface of the medium and were flat or concave on the attachment surface.

Multiple variations in color, shape and size were observed. The resistant bodies were black, dark green or white at first, becoming black with the age; they were flattened, hemispherical, rounded, roughly circular, spongy, regular or irregular in shape, with smooth, nodose or reticulated surface, discrete or confluent, or in agglomeration.

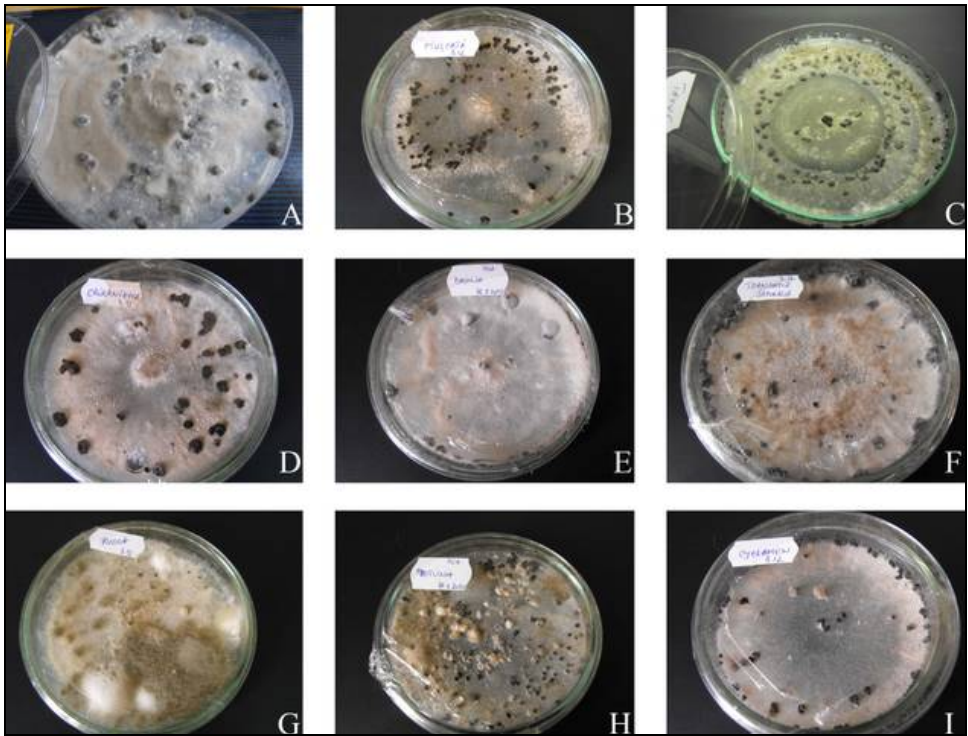


Fig. 4. The distribution and the pattern of sclerotia formation on the surface of PDA medium plates: entire surface (A, B, D, F, G, H, I), concentric rings (C), on the edges of the plates (E) (A – *Rosa* sp., B – *Geranium* sp., C – *Taxus* sp., D – *Chrysanthemum* sp., E – *Dahlia* sp., F – *Hibiscus* sp., G – *Fuchsia* sp., H – *Petunia* sp., I – *Cyclamen* sp.)

Conclusions

The growth rate of the colonies was higher on the PDA medium compared to the Czapek medium, reaching maximum development in five respectively seven days.

Sporulation was also better on PDA; on Czapek medium only two isolates developed spores.

The conidia were ovate, ellipsoidal, globose to subglobose and smooth.

The length of conidia on PDA medium fell in the range of 9.37 μm (*Hibiscus* sp.) and 12.04 μm (*Fuchsia* sp.); the width fell in the range of 7.94 μm (*Taxus* sp.) and 10.2 μm (*Fuchsia* sp.).

On Czapek medium the length values were 11.4 μm for the *Fuchsia* sp. isolate and 10.9 for the *Dahlia* sp. isolate and the width of the spores was 9.5 μm in *Dahlia* sp. and 9.7 μm in *Fuchsia* sp. isolate.

Sclerotia varied in size and shape, with different distribution models: in concentric rings, on the edge of the Petri plate and irregular.

REFERENCES

- Beever, R.E., Weeds, P.L. (2004) Taxonomy and genetic variation of *Botrytis* and *Botryotinia*. In: Elad, Y., Williamson, B., Tudzynski, P., Delen, N. (Eds). *Botrytis: Biology, Pathology and Control*. Kluwer Academic Publisher, Dordrecht, pp. 29-52.
- Constantinescu, O., (1974) *Metode și tehnici în micologie*, Ed. Ceres, București.
- Droby, A., Lichter A. (2004) Post-harvest Botrytis infection: etiology, development and management. In: Elad, Y., Williamson, B., Tudzynski, P. Delen, N. (Eds), *Botrytis: Biology, Pathology and Control*. Kluwer Academic Press, Dordrecht, pp. 349–367.
- Elad, Y., Williamson, B., Tudzynski, P., Delen, N. (2004) *Botrytis* spp. and diseases they cause in agricultural systems- an introduction. In: Elad, Y., Williamson, B., Tudzynski, P. Delen, N. (Eds), *Botrytis: Biology, Pathology and Control*. Kluwer Academic Press, Dordrecht, pp. 1-8.
- Grindle, M., (1979) Phenotypic Differences Between Natural and Induced Variants of *Botrytis cinerea*, *J. Gen. Microbiol.*, **111**, 109-120.
- Váczy, Zsuzsanna, Váczy, K. Z., Karaffa, L., Sándor, Erzsébet (2010) Differences between *Botrytis cinerea* populations causing grey mould and noble rot in two Hungarian vineyards, XV International Botrytis symposium, Cádiz, Spain, pp 38.
- Williamson, B., Bettina Tudzynski, P., Tudzynski, J. A. L., Van Kan (2007) Pathogen profile, *Botrytis cinerea*: the cause of grey mould disease, *Mol. Plant Pathol.*, **8** (5), 561–580.

*** <http://web.aces.uiuc.edu>

THE PHOTOCHEMICAL PS II ACTIVITY IN CYANOBACTERIAL STRAINS BELONGING TO THE NOSTOCALES GROUP IN ANAEROBIOSIS CONDITIONS

VICTOR BERCEA¹, CRISTIAN COMAN¹,
COSMIN SICORA^{1,2,✉} and NICOLAE DRAGOȘ³

SUMMARY. The effect of anaerobiosis on the fluorescence in *Anabaenopsis* sp. AICB 717 and *Aphanizomenon elenkinii* AICB 709 strains was investigated. Chlorophyll *a*, carotenoids and phycobiliproteins, identified based on their absorption spectrum, showed no significant alterations in anaerobiosis conditions. The minimal (F_0) and maximal (F_m) fluorescence yield, decreased in the first 60 min of anaerobiosis, followed by a light increase at the end of the argon treatment. The PS II reaction centers' oxidation/reduction state dropped in intensity in the first moments of anaerobiosis. The PS II maximal quantum yield (F/F_m) and the effective quantum yield ($Y(II)$) showed an increased variability reported to the strain investigated. The photochemical coefficients qP and qL had a similar growth, their value being close to 1, this showing the oxidative redox state of the PS II reaction centers. The photochemical quenching and the quantum yield of nonregulated energy dissipation are at their maximum, designating the fact that there is a weak photochemical conversion of energy caused by the light absorption antenna complex. In the presence of DCMU a weak energization state was recorded, leading to relatively equal F_0 and F_m values caused by the fact that all the PS II reaction centers become closed (reduced) causing a decrease of fluorescence.

Keywords: chlorophyll fluorescence; DCMU inhibitor; photochemical activity; photosystem PS II and PS I; photochemical quenching;

Introduction

Light energy catching by cyanobacteria is undertaken by phycobilisomes which are protein-pigment complexes formed by heterodimeric phycobiliproteins assembled with the help of polipeptides in order to absorb light and send it to the reaction centers of PS II. These complexes are associated with the surface of the

¹ Institute of Biological Research, 48 Republicii Street, 400015/Cluj-Napoca, România.
E-mail: bercea_victor@yahoo.com

² Biological Research Center, Parcului Street, no.14, 455200/Jibou, Sălaj County, România.

³ Faculty of Biology and Geology, Babeș-Bolyai University, 5-7 Clinicilor Street, Cluj-Napoca, România.

✉ **Corresponding author: Cosmin Sicora**, Institute of Biological Research, 48 Republicii Street, 400015/Cluj-Napoca, România. E-mail: cosmin.sicora@gmail.com

thylakoidal membrane (Arteni *et al.*, 2009). The phycobiliproteins concure to fluorescence because they overlap the chlorophyll's emission spectrum thus influencing the minimal fluorescence (Campbell *et al.*, 1998; Cruz *et al.*, 2005).

The fluorescence is modulated by the oxidoreductive state of the primary acceptor Q_A . When Q_A is oxidized the minimal level of fluorescence is achieved, while the fluorescence reaches its maximal level when Q_A is completely reduced (Bissati *et al.*, 2000).

In anaerobic and dark conditions cyanobacteria produce hydrogen, the hydrogenase genes are expressed and the hydrogenase takes the electrons from the photosynthetically reduced ferredoxin (Beneman, 2000). Photosynthetic microorganisms can produce hydrogen in the presence of light also and this shows that the fundamental process in understanding the photobiologically H_2 production is the photosynthesis, which uses solar energy (Levin *et al.*, 2004; Melis, 2007; Prince and Kheshgi, 2005).

In this study the kynetics of the chlorophyll fluorescence induction is presented for strains of cyanobacteria belonging to the Nostocales group, in anaerobic conditions.

Material and method

The *Anabaenopsis* sp. AICB 717 and *Aphanizomenon elenkinii* AICB 709 cyanobacterial strains, belonging to the Nostocales group, were grown at ambient temperature, on GZ culture medium, in air bubbling and continous light at the intensity of $28 \mu\text{mol. m}^{-2} \cdot \text{s}^{-1}$. The growth period was 10 days and the culture was in its exponential phase at the time of argon (1 bar) treatment. The culture was bubbled with argon for 2 hours in order to create the anaerobic state, the chlorophyll fluorescence being measured at 40, 60 and 120 min intervals using the Walz-100 fluorometer, from samples accomodated to dark for 30 min. In both control and anaerobic samples the photochemical activity of the PS II photosystem was measured in the presence of $10 \mu\text{M}$ DCMU (3-(3,4-diclorofenil)- 1,1-dimetilurea). Other parameters determined were the content of chrrophyll a (Arnon, 1949) and carotenoids, based on specific absorption coefficients, their identification being carried out based on the maximal peak of absorption observed using a Jasco V-630 spectrophotometer.

Results and discussion

A. The PS II photosystem activity study in Anabaenopsis sp. AICB 717 based on the chlorophyll fluorescence

The *in vivo* absorption of the *Anabaenopsis* sp. AICB 717 culture, with an optical density of $OD_{680} = 0.576$, highlighted the spectral absorption areas for the constituents of the photosynthetic apparatus (Fig. 1). In the blue spectral zone, between 400-500 nm, the carotenoids and the chlorophyll a absorb, and in the red spectral zone, between 620-700 nm, the phycobilins (621 nm) and the chlorophyll a absorb (680 nm). No *in vivo* spectral changes were observed after inducing the anaerobic state in the cell suspensions.

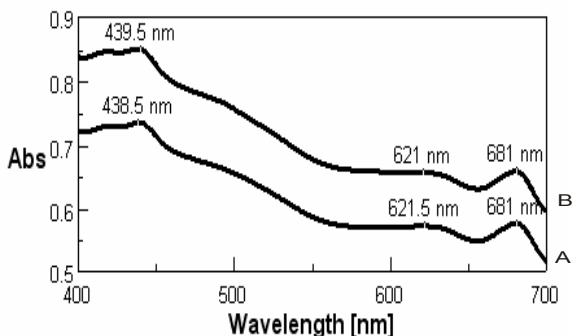


Fig. 1. The *in vivo* absorption spectrum of the *Anabaenopsis* sp. AICB 717 culture, **A:** at the beginning of the argon treatment (control); **B:** after the treatment (end).

The concentration of the assimilating pigments remained in an equilibrium state during anaerobiosis by argon bubbling (Table 1).

Table 1.

Quantity of assimilating pigments in *Anabaenopsis* sp. AICB 717 (mg/l)

Pigments (mg/l)	Control	Anaerobiosis
chlorophyll <i>a</i>	1,113	1,1
Total carotenoids	0,413	0,443
<i>a</i> /carotenoids	2,69	2,48
Total assimilating pigments	1,526	1,543

Generally, the environmental factors can disturb the equilibrium between entrance and consumption of energy in the photosynthetic apparatus by inducing certain mechanisms that maintain the equilibrium (Maxwell *et al.*, 1994).

In the *Anabaenopsis* sp. AICB 717 suspension the minimal (F_0) and maximal (F_m) fluorescence have decreased with a tendency to increase at the end of the argon treatment (Fig. 2). F_0 decreased in anaerobiosis because the energy is not available to photosystems and the reaction centers are totally open (oxidized), ready to absorb light. In these conditions, the photochemical conditions prevail, while the NPQ processes are minimal. F_m is a measure of the closing state of the PS II photosystem reaction centers (reduced state) and expresses the condition in PS II when Q_A , the primary electron receptor in PS II, is entirely reduced. A similar evolution was recorded for the variable fluorescence (F_v), whose real values were pretty low following the close values of F_0 and F_m . The decrease of F_0 and F_m values implies a mechanism that is tied to the dissipation of absorbed in the PS II antennary complex (Verhoeven *et al.*, 1996).

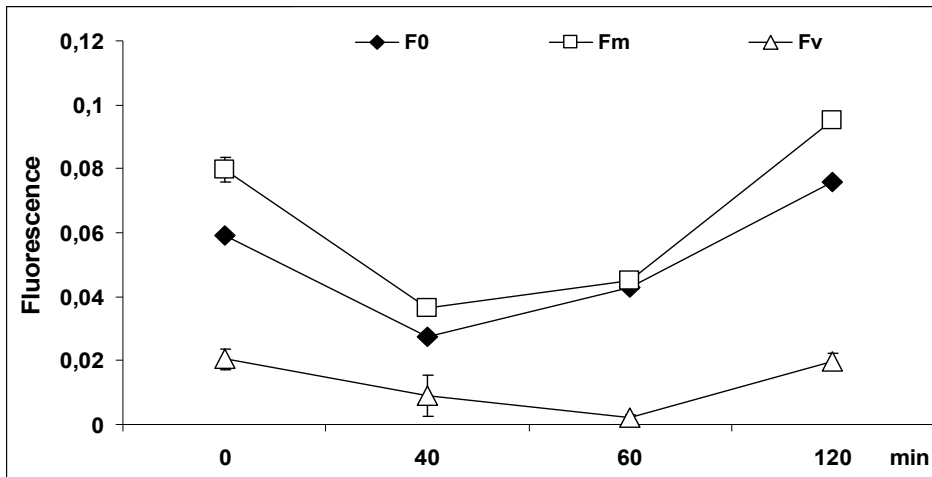


Fig. 2. The evolution of the minimal (F_0) and the maximal (F_m) fluorescence in PS II after the argon treatment (120 min) compared to control (0 min).

The maximal quantum yield or the efficiency of the PS II photosystem, measured by the relation F/F_m , was maintained slightly higher compared to control, but dropped at the end of anaerobic conditions (Fig. 3). The mean value of 0.7 for the F/F_m ratio shows a high efficiency in the quantum yield of the photochemistry of PS II which certifies that all the reaction centers are open and the unphotochemical dissipation of the excitation energy (NPQ) is 0. The theoretical value of F/F_m is around 0.832 and the 1 value is not reached as a consequence of the increase of F_0 following a blockage in the PS II reaction centers, fact due to the turnover of the D_1 protein.

The effective PS II quantum yield (Y_{II}) decreased during the argon treatment (Fig. 3). The quantum yield of nonregulated energy dissipation (Y_{NO}) showed high values in the first 60 min of anaerobiosis with a tendency to decrease at the end of the treatment. The Y_{NO} values were approximately the same with those of F/F_m . The quantum yield of regulated energy dissipation (Y_{NPQ}) was 0.

The photochemical coefficient qP (which is a measure of the open reaction centers) increased in anaerobiosis conditions as compared to control (Fig. 4). The coefficient of the photochemical quenching qL , which is a real measure of the open reaction centers, presented a similar evolution. The high value of qL expresses the usage of the excitation energy during photochemistry in the reaction centers, and the fluorescence is reduced. The excitement pressure and the energy dissipation through NPQ were 0. The reduction of the transfer energy efficiency towards the PSII reaction centers leads to the reduction of the PS II antenna size and to a decrease in the photosynthetic efficiency highlighted in the quantum yield (Huner *et al.*, 1998).

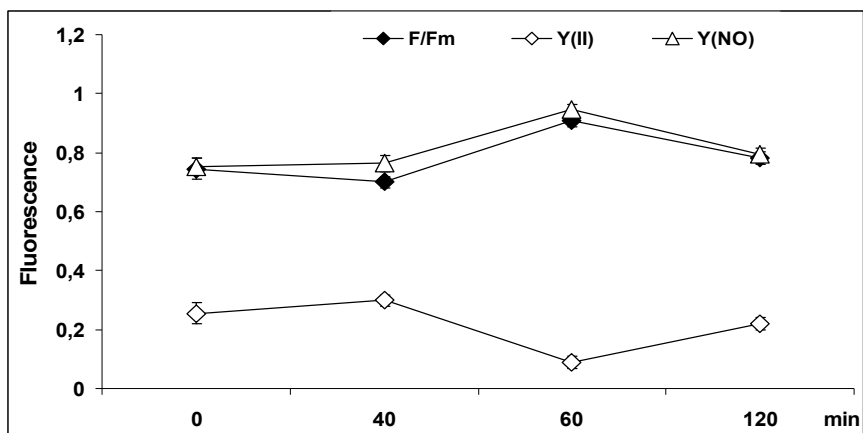


Fig. 3. The PS II quantum yields' evolution during argon treatment (120 min) compared to control (0 min).

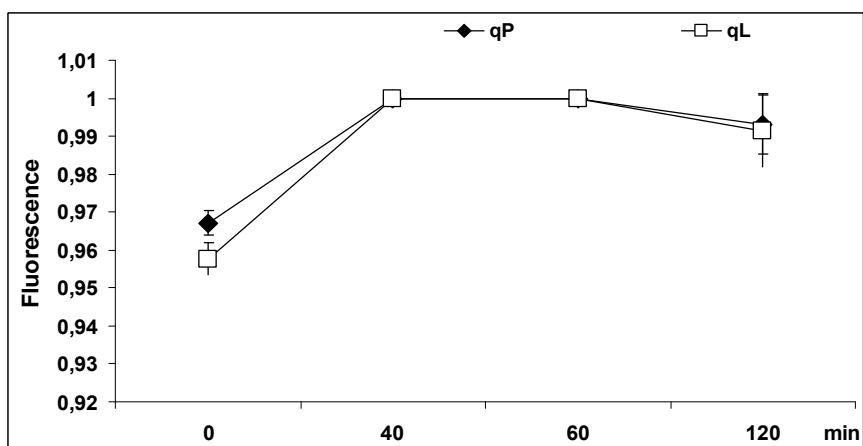


Fig. 4. The PS II qP and qL photochemical coefficients' evolution during argon treatment (120 min) compared to control (0 min).

The fluorescence induction kinetics through the saturation pulse showed a relative normal evolution of the fluorescence parameters in the control sample (Fig. 5). The F_0 and F_m fluorescence level as well as the difference between them after the first saturation impulse in the sample are obvious for the PS II, related to the PS I photosystem activity. Both photosystems are structures incorporated in the thylacoidal membrane and work in series. The kinetics of the induction curve in the light-dark interval by analyzing the saturation pulse shows decreased values of the PS II fluorescence parameters. After the first saturation pulse of oversaturated light, the F_m level is increasing in the illuminated samples.

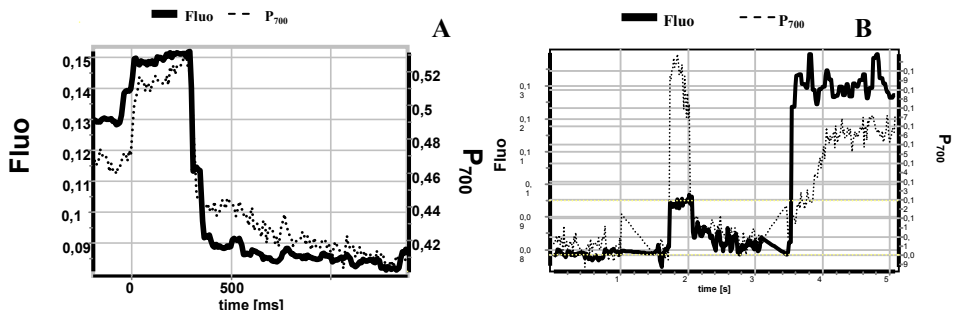


Fig. 5. The fluorescence kinetics (A) and curve kinetics (B) induction through the saturation pulse for the control sample of *Anabaenopsis* sp. AICB 717: PS II fluorescence (Fluo) compared to the PS I activity (P700).

At the end of the argon treatment, the fluorescence induction kinetics by analyzing the light saturation pulse underlined the reestablishment of the fluorescence parameters level, which reach a normal stage (Fig. 6).

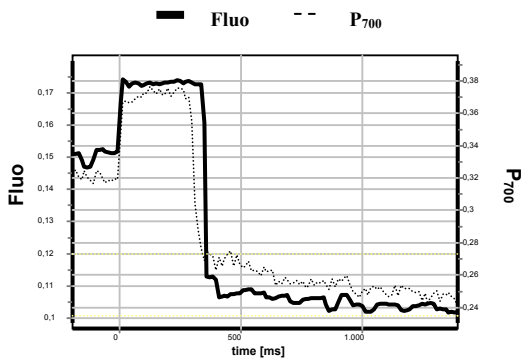


Fig. 6. The pulse saturation chlorophyll fluorescence kinetics of *Anabaenopsis* sp. AICB 717 at the end of the argon treatment: PS II fluorescence (Fluo) compared to the PS I activity (P700).

In the presence of the DCMU (3-(3,4-dichlorophenyl)-1,1-dimethylurea), which inhibits the electron transfer from the PS II reaction centers to the plastoquinone (PQ), F_0 and F_m end up to be of almost equal value due to the fact that all the PS II reaction centers become closed (reduced), this leading to a decrease of the variable fluorescence (F_v), which showed negative values (Fig. 7). In the presence of DCMU, the effective PS II quantum yield (Y_{II}) has reduced significantly and the quantum yield of nonregulated energy dissipation (Y_{NO}), as well as the the coefficient of photochemical quencing q_L , have increased (Fig. 7). The q_P and q_L coefficients reported values near to 1, which certifies the reduced fluorescence intensity as a result of the fact that the excitement energy is effectively converted in the photochemical reactions.

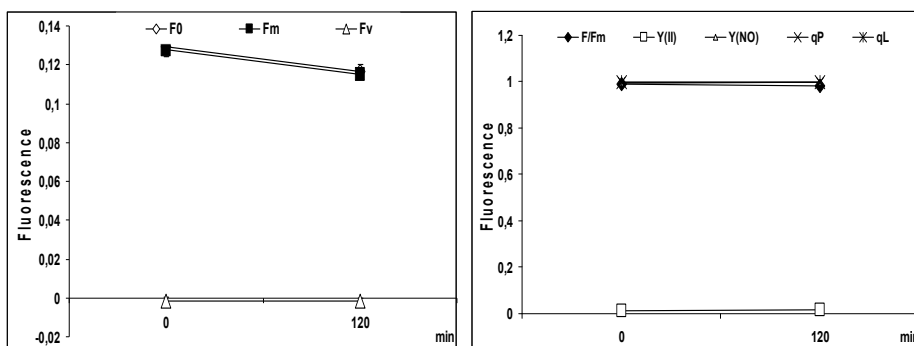


Fig. 7. The evolution of PS II fluorescence parameters in the presence of DCMU under argon treatment (120 min) compared to control (0 min).

B. The PS II photosystem activity study in *Aphanizomenon elenkinii* AICB 709 based on the chlorophyll fluorescence

The *in vivo* spectra of the *Aphanizomenon elenkinii* AICB 709 culture highlighted the absorbance for chlorophyll *a* (420 nm, 439 nm) and carotenoids (490 nm), and in the red spectral zone the absorbance of phycobilins (595 nm, 635 nm) and chlorophyll *a* (681 nm) (Fig. 8).

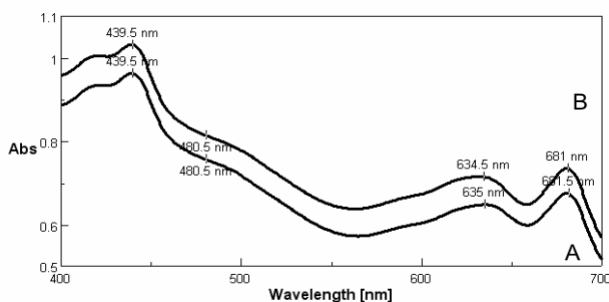


Fig. 8. The *in vivo* absorption spectrum of the *Aphanizomenon elenkinii* AICB 709 culture, **A:** at the beginning of the argon treatment (control); **B:** after the treatment (end).

The components of the photosynthetic apparatus are presented in table 2: the pigment concentration is quite low with no significant differences between the control and the suspensions treated with argon.

The minimal chlorophyll fluorescence in *Aphanizomenon elenkinii* AICB 709 showed very low values, being relatively close to the maximal fluorescence values F_m which indicates that not all the reaction centers are open. Under the argon treatment, F₀ decreased during the 60 min of anaerobiosis (Fig. 9). At the end of the 120 min of argon treatment, the F₀ level has restored to values similar to control. The maximal chlorophyll fluorescence (F_m) presented a similar evolution. The approximate equal values of F₀ and F_m led to obtaining some very low values of variable fluorescence F_v.

Table 2.

Quantity of assimilating pigments in *Aphanizomenon elenkinii* AICB 709 (mg/l)

Pigments (mg/l)	Control	Anaerobiosis
chlorophyll a	1,625	1,745
Total carotenoids	0,440	0,502
a/carotenoids	3,69	3,47
Total assimilating pigments	2,065	2,247

The increased level of F_0 is due to the high ratio between phycocyanin and chlorophyll. The F_0 level varies together with the concentration of phycobiliproteins. The F_m is reached after exposure to light when the plastoquinone nucleus shifts to the first redox state (oxidation). The cells adapted to dark have the plastoquinone nucleus in its reduced state, the second redox state with a reduced fluorescence emission for PS II. The surplus of energy absorbed in phycobilisomes is dissipated in the form of heat, this way the energy that ends up in the reaction center is reduced. The spread of energy consists in the reduction of fluorescence. This mechanism involves the carotenoid binding proteins (Boulay *et al.*, 2008).

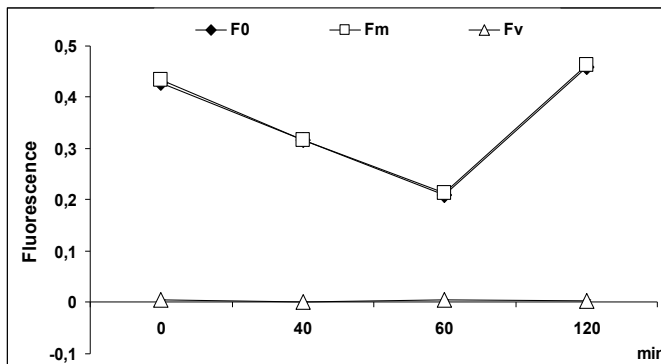


Fig. 9. The minimal (F_0), maximal (F_m) and variable PS II fluorescence evolution under argon treatment (120 min), compared to control (0 min).

The maximal PS II quantum yield (F/F_m) and the quantum yield of nonregulated energy dissipation (Y_{NO}) presented higher values (Fig. 10). After adapting to darkness, normally the PS II reaction centers are open ($F=F_0$), the unphotochemical energy dissipation is minimal ($q_N=NPQ=0$) and the maximal quantum yield F_m is reached through the saturation pulse. During anaerobiosis induced by argon treatment the values did not change significantly in comparison with the control.

The effective PS II quantum yield Y_{II} showed very low values, and the quantum yield of regulated energy dissipation (Y_{NPQ}) was zero. The quantum yield of nonregulated energy dissipation $Y_{(NO)}$ recorded pretty high values which underlines a more reduced efficiency in the photochemical conversion of energy.

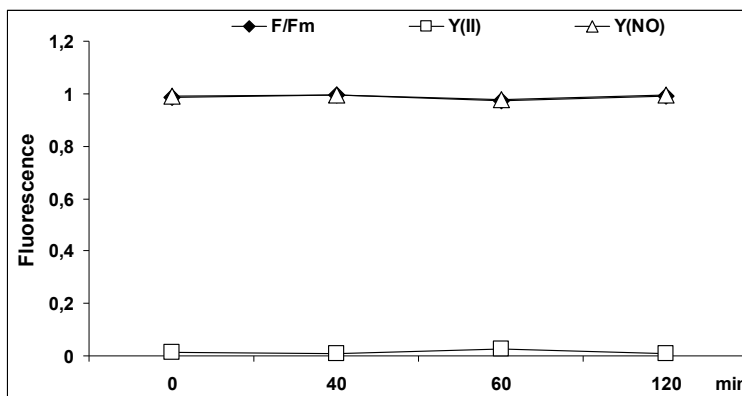


Fig. 10. The PS II quantum yields' evolution under argon treatment (120 min), compared to control (0 min).

The evolution of the coefficient of photochemical quenching is presented in Fig. 11. The q_L coefficient, which is a measure of the open PS II reaction centers, and the q_P photochemical coefficient, which is a measure of PS II units capable of reducing the plastoquinone, have shown values close to 1 (the maximal theoretic value). No differences between the control and the argon induced anaerobiosis were observed.

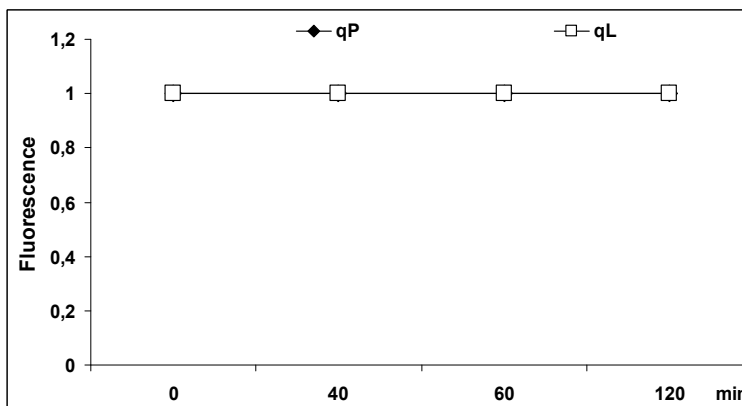


Fig. 11. The PS II q_P and q_L photochemical coefficients' evolution under argon treatment (120 min) compared to control (0 min).

Pulse saturation fluorescence induction kinetics showed a relatively close and high level of the minimal and maximal fluorescence parameters (Fig. 12). At the end of the argon treatment (120 min), the pulse saturation fluorescence induction kinetics is showing a disequilibrium among the fluorescence parameters and the redox state of the PS II reaction centers, which are entirely open after applying a light saturation pulse, this leading to a very low minimal fluorescence F_0 .

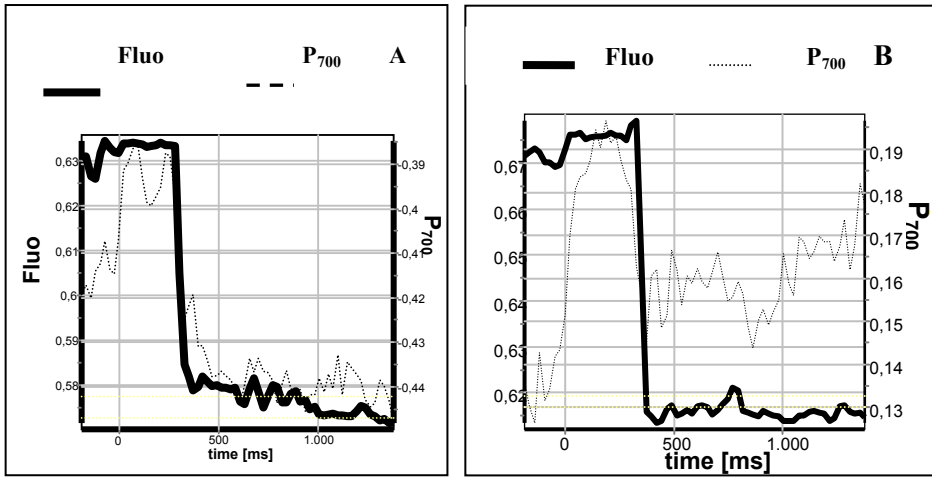


Fig. 12. The pulse saturation fluorescence induction kinetics for *Aphanizomenon elenkinii* AICB 709: **A** – control and **B** - at the end of anaerobiosis conditions PS II fluorescence (Fluo) and PS I activity (P₇₀₀).

In the presence of the DCMU (3-(3,4-dichlorophenyl)-1,1-dimethylurea) inhibitor, F_0 and F_m showed relatively high and close values which highlights the closed state of the PS II reaction centers (Fig. 13). The variable fluorescence dropped to negative values which explains the inactivation state of the PS II photosystem reaction centers. The photochemical efficiency (F/F_m) and the quantum yield of the unregulated energy dissipation $Y_{(NO)}$ increased to maximum. The effective quantum yield of PS II photosystem, $Y_{(II)}$, dropped to minimum. DCMU, a compound that inhibits the reoxidation of Q_A through Q_B , causes the shutdown of the reaction centers (Boussac *et al.*, 2011).

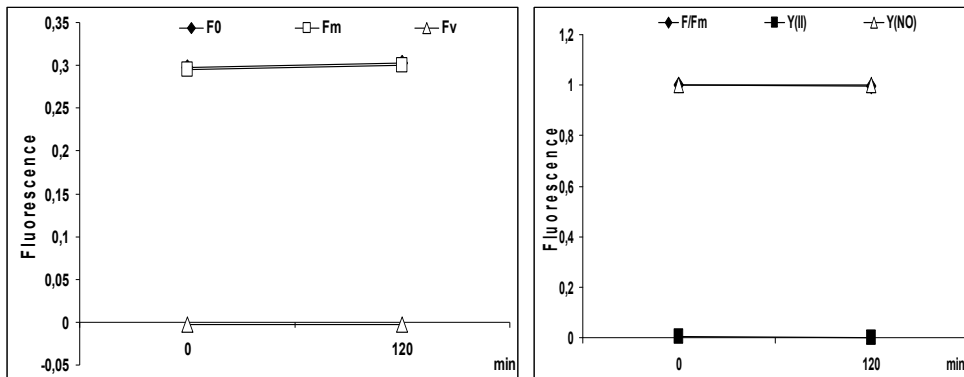


Fig. 13. The evolution of the PS II fluorescence parameters in the presence of DCMU under the argon treatment (120 min), compared to control.

The photochemical coefficient qP (the estimated measure of the open reaction centers) grew in anaerobiosis conditions compared to control (Fig. 14). The photochemical quenching coefficient qL , which is the real measure of the open reaction centers, had a similar evolution.

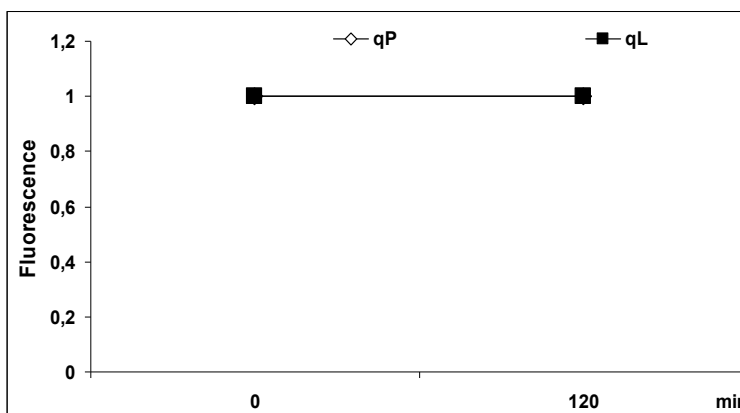


Fig. 14. The PS II photochemical coefficients' evolution in the presence of DCMU under the argon treatment (120 min), compared to control (0 min).

When the electron flow is inhibited by DCMU, the fluorescence curve reflects only the photochemical events, leading to a complete reduction state of QA (Haldimann and Tsimilli-Michael, 2005).

Conclusions

The results obtained in regards to the effect of anaerobiosis on the activity of the PS II photosystem are reported to the dynamics of the chlorophyll's fluorescence and photosynthetic components specific to each cyanobacterial strain belonging to the nostocales group.

- The components of the photosynthetic apparatus, like chlorophyll a, carotenoids and phycobiliproteins, identified based on their absorption spectrum, showed no significant alterations in anaerobiosis conditions, as compared to control.

- The PS II photosystem's activity, which was monitored through the minimal (F_0) and maximal (F_m) fluorescence yield, decreased in the first 60 min of anaerobiosis, followed by a light increase at the end of the argon treatment. An exception was the *Aphanizomenon elenkinii* AICB 709 strain for which equal F_0 and F_m values were observed due to the fact that the PS II reaction centers were not fully opened. The PS II reaction centers' oxidation/reduction state dropped in intensity in the first moments of anaerobiosis.

- The PS II maximal quantum yield (F/F_m) and the effective quantum yield (Y_{II}) showed an increased variability reported to the strain investigated. Generally, the quantum yield increased at the beginning and decreased at the end of the argon treatment. The quantum yield of nonregulated energy dissipation (Y_{NO}) appeared intensely during the treatment. The photochemical coefficients qP and qL had a similar growth, their value being close to 1, this showing the oxidative redox state of the PS II reaction centers. The photochemical quenching and the quantum yield of nonregulated energy dissipation are at their maximum, designating the fact that there is a weak photochemical conversion of energy caused by the light absorption antenna complex. The oscillations of the oxidation/reduction states are well highlighted by the fluorescence induction kinetics and by the fluorescence curve.

- In the presence of DCMU, which inhibits the electron transfer from the PS II reaction centers to plastoquinone, a weak energization state was recorded, leading to relatively equal F_0 and F_m values caused by the fact that all the PS II reaction centers become closed (reduced) causing a decrease of the variable fluorescence (F_v). The PS II photosystem's photochemical efficiency and the effective quantum yield decreased, while the quantum yield of nonregulated energy dissipation $Y_{(NO)}$ increased together with the coefficients of photochemical quenching. The effect of DCMU explains the heterogeneity of the PS II photosystem's antenna: there are energy consumption restrictions at the PS II level regarding the excitation transfer. DCMU helps to totally close the reaction centers.

Acknowledgements

This research was supported by POS-CCE Program nr. 236/16.08.2010.

REFERENCES

- Arnon, D. (1949) Copper enzymes in isolated chloroplasts. Polyphenoloxidase in *Beta vulgaris*. *Plant Physiol.*, **24** (1), 1-15.
- Arteni, A. A., Ajlani, G., Boekema, E. J. (2009) Structural organisation of phycobilisomes from *Synechocystis* sp. strain PCC6803 and their interaction with the membrane. *Biochim. Biophys. Acta*, **1787**, 272-279.
- Benemann, J. R. (2000). Hydrogen production by microalga. *J. Appl. Phycol.*, **12**, 291-300.
- Bissati, K. E., Delphin, E., Murata, N., Etienne, A. L., Kirilovsky, D. (2000) Photosystem II fluorescence quenching in the cyanobacterium *Synechocystis* PCC 6803: involvement of two different mechanisms. *Biochim. Biophys. Acta*, **1457**, 229-242.

- Boulay, C., Abasov, L., Six, C., Vass, I., Kirilovsky, D. (2008) Occurrence and function of the orange carotenoid protein in photoprotective mechanisms in various cyanobacteria. *Biochim. Biophys. Acta*, **1777**, 1344-1354.
- Boussac, A., Sugiura, M., Rappaport, F. (2011) Probing the quinone binding site of photosystem II from *Thermosynechococcus elongatus* containing either PsbA₁ or PsbA₃ as the D₁ protein through the binding characteristics of herbicides. *Biochim. Biophys. Acta*, **1807**, 119-129.
- Campbell, D., Hurrz, V., Clarke, A. K., Gustafsson, P., Öquist, G. (1998). Chlorophyll fluorescence analysis of cyanobacterial photosynthesis and acclimation. *Microbiol. Mol. Biol. Rev.*, **62** (3), 667-683.
- Cruz, J. A., Avenson, T. J., Kanazawa, A., Takizawa, K., Edwards, G. E., Kramer, D. M. (2005) Plasticity in light reactions of photosynthesis for energy production and photoprotection. *J. Exp. Bot.*, **56** (411), 395-406.
- Haldimann, P., Tsimilli-Michael, M. (2005) Non-photochemical quenching of chlorophyll *a* fluorescence by oxidised plastoquinone: new evidences base don modulation of the redox state of the endogenous plastoquinone pool in broken spinach chloroplasts. *Biochim. Biophys. Acta*, **1706**, 239-249.
- Huner, N. P. A., Öquist, G., Sarhan, F. (1998) Energy balance and acclimation to light and cold. *Trends Plant Sci.*, **3**, 224-230.
- Levin, D. B., Pitt, L., Love, M. (2004) Biohydrogen production: prospects and limitations to practical application. *Int. J. Hydrogen Energy*, **29**, 173-185.
- Maxwell, D. P., Falk, S., Trick, C. G., Huner, N. P. A. (1994) Growth at low temperature mimics high-light acclimation in *Chlorella vulgaris*. *Plant Physiol.*, **105**, 535-543.
- Melis, A. (2007). Photosynthetic H₂ metabolism in *Chlamydomonas reinhardtii* (unicellular green algae). *Planta*, **226**, 1075-1086.
- Prince, R. C., Kheshgi, H. S. (2005) The photobiological production of hydrogen: potential efficiency and effectiveness as a renewable fuel. *Crit. Rev. Microbiol.*, **31**, 19-31.
- Verhoeven, A. S., Adams III, W. W., Demmig-Adams, B. (1996) Close relationship between the state of the xanthophyll cycle pigments and photosystem II efficiency during recovery from winter stress. *Physiol. Plant.*, **96**, 567-576.

THE EFFECT OF ARGON-INDUCED ANAEROBIOSIS ON THE ACTIVITY OF PHOTOSYSTEM PS II IN SOME NOSTOCALES SPECIES

VICTOR BERCEA¹, ADRIANA BICA¹, BOGDAN DRUGĂ¹,
COSMIN SICORA^{1,2,✉} and NICOLAE DRAGOȘ³

SUMMARY. The effects of atmospheric gases with anaerobiosis induction on the photosystem PS II activity at *Nostoc linckia* AICB 421 and *Cylindrospermum alatosporum* AICB 39 strains are related to the dynamics of the chlorophyll fluorescence and to the photosynthetic compounds, specific to each cyanobacterial strain. The minimal fluorescence (F_0) and maximal fluorescence (F_m) decreased in the first 60 min, followed by a slightly increase at the end of the argon treatment. The maximal quantum yield of the PS II (F/F_m) and the effective PS II quantum yield (Y_{II}) recorded a large variability. The quantum yield of nonregulated energy dissipation (Y_{NO}) was highly intense during the treatment. The high values of the coefficients of photochemical quenching qP and qL assess the oxidative redox state of the reaction centres PS II. The photochemical quenching and the quantum yield of the non-regulated energy recorded maximal values, which indicate that a poor photochemical conversion of the energy exists at the light-harvesting antenna complex. In DCMU presence, a poor energizing state was recorded, because all the reaction centres PS II are closed (reduced), resulting in a decrease of the variable fluorescence (F_v). In DCMU presence, the fluorescence rate is dependent of the functional size of the antenna PS II.

Keywords: chlorophyll fluorescence; DCMU inhibitor; photochemical activity; photosystem PS II and PS I; photochemical quenching.

Introduction

Cyanobacteria are photosynthetic organisms which lack chlorophyll *b*, but detain phycobilisomes which are light-harvesting complexes, located at the surface of the thylacoid membrane. Cyanobacteria detain a unique way for transferring the energy to the photosystem antenna. In cyanobacteria, all chlorophylls are located only within the core of the antenna of PS I and PS II: chlorophylls/ P_{700} ratio is 100 and that of chlorophylls/ P_{680} is 40. Chlorophylls with high wavelengths transfer the

¹ Institute of Biological Research, 48 Republicii Str., 400015/Cluj-Napoca, România.
E-mail: bercea_victor@yahoo.com

² Biological Research Center, 14 Parcului Street, 455200/Jibou, Sălaj County, România.

³ Faculty of Biology and Geology, Babeș-Bolyai University, 5-7 Clinicilor Str., Cluj-Napoca, România.

✉ **Corresponding author: Cosmin Sicora**, Institute of Biological Research, 48 Republicii Street, 400015/Cluj-Napoca, România. E-mail: cosmin.sicora@gmail.com

energy to the P₇₀₀ reaction centre, but are involved in the energy excess dissipation when PS I reaction centres are accumulated in a reduced, oxidized or triplet state. When the accepting side of the PS I is in reduced state, the electron transport is blocked, the charges recombination leads to the P₇₀₀ triplet formation and the fluorescence decreases. In both cases, the absorbed energy can not be used in the reaction centres, and the fluorescence decrement may be considered as nonphotochemical quenching. Carotenoids are responsible for the fluorescence reduction, induced by blue light at the phycobilisomes level (Karapetyan, 2007). The fluorescence variation results from the variable interaction between the phycobilisomes and the two photosystems, PS II and PS I (Krause and Weis, 1991).

The variability of the excitation spectrum of cyanobacteria comes from the adaptation mechanism of the photosynthetic apparatus in different environmental conditions. The light and nutrients induce changes in the phycocyanine content of the phycobilisomes, modifying the optical absorption of the light-harvesting complexes (LHC) (Beutler *et al.* 2003).

In anaerobic and dark conditions, cyanobacteria produce H₂ (Beneman, 2000). Photosynthetic microorganisms may produce hydrogen in light conditions, which shows that the fundamental process of understanding hydrogen synthesis is photosynthesis which uses the energy of light (Levin *et al.*, 2004; Melis, 2007; Prince and Kheshgi, 2005).

The present study presents the anaerobiosis effect on the kinetics of the chlorophyll fluorescence induction in cyanobacteria from Nostocales species.

Materials and methods

Cyanobacteria *Nostoc linckia* AICB 421 and *Cylindrospermum alatosporum* AICB 39 have been cultivated at room temperature, on GZ medium, continuously air supplied, under medium intensity light of 28 μmol. m⁻².s⁻¹. After 10 days growth period, when the suspension reached exponential phase, the argon treatment (1 bar) was applied for 2 hours to induce the anaerobiosis conditions and the chlorophyll fluorescence measurements were taken at 40, 60 and 120 min intervals contribution of PS I to F₀ was subtracted from the measured quantity of fluorescence. using a PAM-100 fluorometer on samples kept in dark for 30 min. The 30% presence of DCMU (3-(3,4-dichlorophenyl)-1, 1-dimethylurea) also, using control probes and those subjected to treatment with argon. The results represent the mean of 5 repetitions.

Results and discussion

A. The study of the PS II photosystem activity based on the chlorophyll fluorescence in *Nostoc linckia* AICB 421.

The activity of photosystem PS II, highlighted by the measurement of chlorophyll fluorescence in anaerobiosis conditions is shown in Fig. 1. The minimal fluorescence (F₀), the maximal fluorescence (F_m) and the variable fluorescence (F_v)

also, recorded normal values which relate to the cell suspension density and to the chlorophyll a quantity. In the first 40 minutes of anaerobiosis the F_o and F_m level decreased, followed by an increased progression. F_v continued to decrease towards the end of the argon treatment. The photochemical efficiency of PS II (F/F_m), considered quite high as real value, recorded a relatively proportional increase during anaerobiosis, similarly with that observed for the quantum yield of nonregulated energy dissipation (Y_{NO}). The effective PS II quantum yield (Y_{II}) recorded low values which gradually decreased during anaerobiosis. The quantum yield of regulated energy (Y_{NPQ}) was zero.

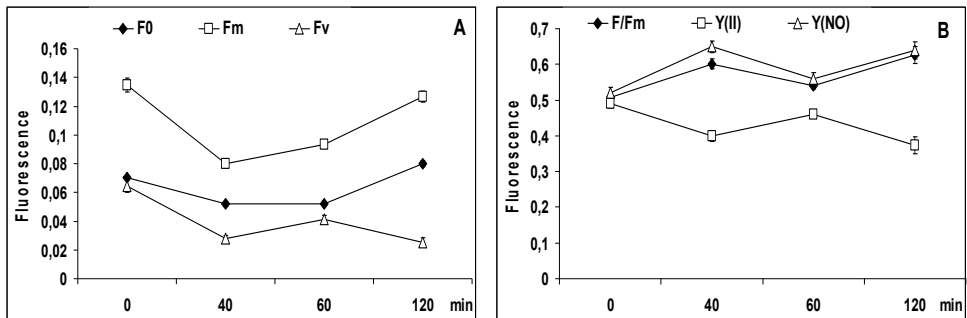


Fig. 1. The minimal (F_o), maximal (F_m), variable (F_v) fluorescence evolution (A) and the quantum yield of the PS II (B) under argon treatment (120 min), compare with the control (0 min).

If the effective PS II quantum yield is significantly reduced, and the photochemical quenching (qP) and the quantum yield of unregulated energy dissipation are maximal, then there is a weak photochemical conversion of the energy, and the causes are at the level of the light-harvesting antenna complex.

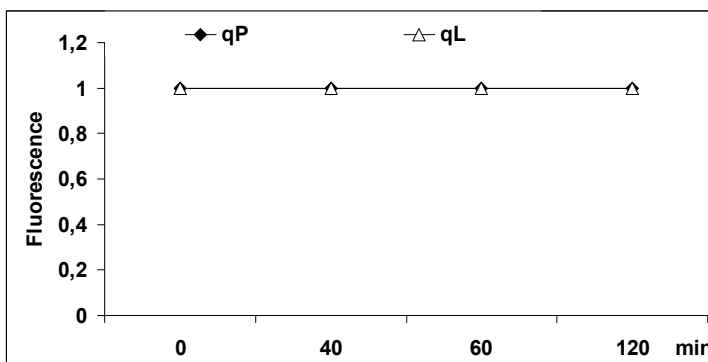


Fig. 2. The evolution of the coefficient of photochemical quenching qP and qL of PS II, under argon treatment (120 min), compare with the control (0 min).

The fluorescence induction by the analysis of the saturation pulse at the control probe, highlighted the low oxidation state of the acceptor side, and after the light pulse the reoxidation reaches high values (Fig. 3). The kinetics of the induction curve shows the high proportion of the opened centres which determine the decrement of F_0 , and after the first light saturation pulse, the closure of the reaction centres PS II occurs rapidly and gradual lowering of F_m takes place, followed by the reaction at the second saturation pulse.

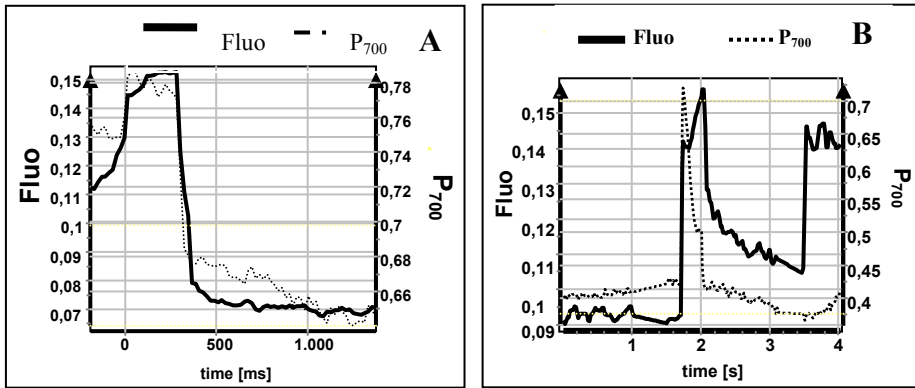


Fig. 3. The kinetics of the fluorescence induction (A) with saturation pulse at *Nostoc linckia* AICB 421, in control and the induction curve (B); PS II fluorescence (Fluo) and the photosystem PS I activity (P_{700}).

At the end of the argon treatment period, the kinetics of the fluorescence induction recorded the increasing of the fluorescence yield followed by a two-phase decay (Kautsky effect). Through the reoxidation due to other light pulses, the fluorescence yield increases, reaching a stable reduction state (Fig. 4). F_0 shows that all the reaction centres are in the opened state (active), and by F_m , all Q_A are reduced and no charge separation occurs (the closure of the reaction centres).

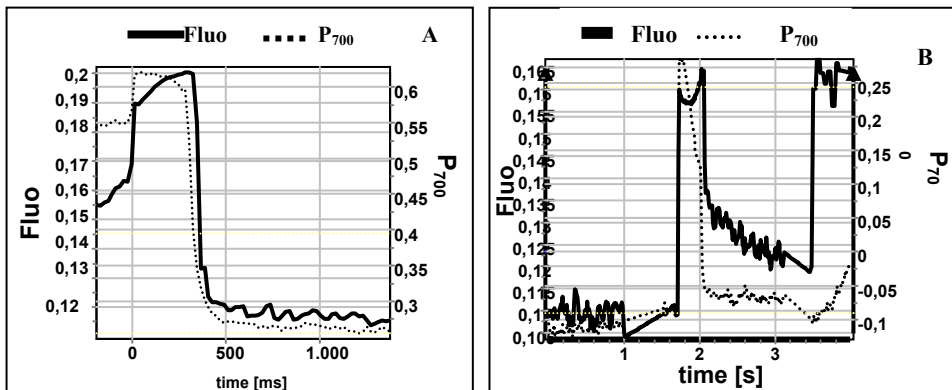


Fig. 4. The kinetics of the fluorescence induction by the saturation pulse in *Nostoc linckia* AICB 421 at the end of the anaerobiosis conditions (A) and that of the induction curve (B); PS II fluorescence (Fluo) and the photosystem PS I activity (P_{700}).

The induction curve, emission from F_0 to F_m reflects the reduction of Q_A . *In vivo*, most of the chlorophyll fluorescence emanates from the antenna system. The closure of reaction centres PS I does not contribute to the variable fluorescence.

In the presence of DCMU inhibitor (3-(3,4-dichlorophenyl)-1, 1-dimethylurea), the chlorophyll fluorescence of the photosystem PS II, in conditions of anaerobiosis, registered a weak state of energizing, leading to relative equal values between F_0 and F_m , causing the reduction of F_v (Fig. 5). The quantum efficiency of PS II (F/F_m) and the quantum yield of nonregulated energy dissipation (Y_{NO}) reached maximal values which demonstrate a poor conversion of the excitation energy, and the effective quantum yield of the reaction centres PS II (Y_{II}) significantly decreased in the presence of DCMU.

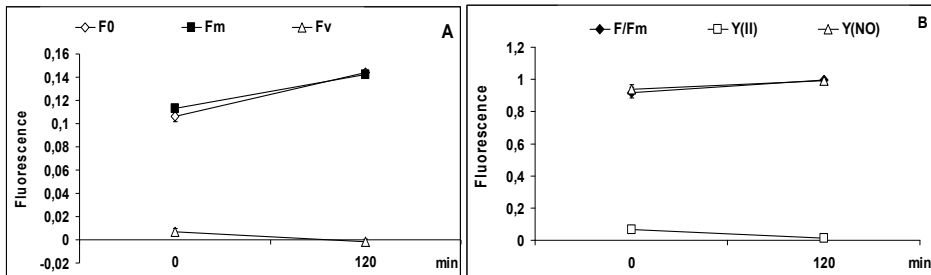


Fig. 5. The evolution of the fluorescence parameters PS II (A) and the quantum yield (B) in control (0 min) and under argon treatment (120 min) in the presence of DCMU.

The photochemical coefficient qP and the quenching coefficient qL recorded a slightly decrement in conditions of anaerobiosis and in the presence of DCMU, attending the dominant oxidative state of the antenna complexes of the photosystem PS II (Fig. 6).

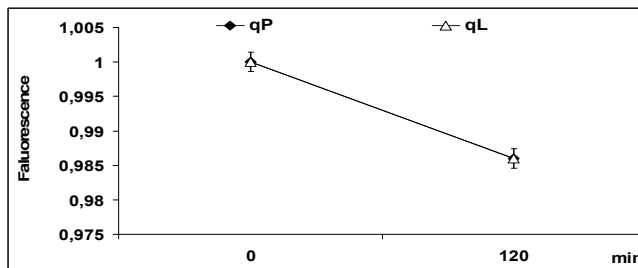


Fig. 6. The evolution of the coefficient of photochemical quenching of PS II in control (0 min) and under argon treatment (120 min) in DCMU presence.

B. Study of the PS II photosystem activity based on the chlorophyll fluorescence in *Cylindrospermum alatosporum* AICB 39

The fluorescence emission of PS II presented relatively normal yields for F_0 and F_m (Fig. 7). F_0 and F_m significantly decreased in the first 60 min of anaerobiosis which produced the lowering of the variable fluorescence (F_v). The decrement of

the chlorophyll fluorescence in photosynthetic apparatus, *in vivo*, is determined by the molecular regulating mechanism directly associated with the excitation transfer of the charges in the reaction centre of PS II, a process which depends on the presence of the xanthophyll pigments (Grudziński *et al.*, 2002).

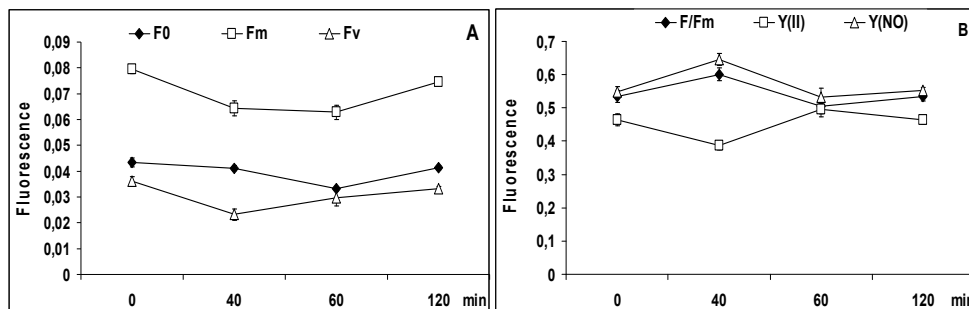


Fig. 7. The minimal (F_0), maximal (F_m) and variable (F_v) fluorescence progression (A) and the quantum yield of PS II (B) under argon treatment (120 min), compare with the control (0 min).

The heterogeneity level of the photosystem PS II is high, and involves changes in the oxidative and reductive sides, within the structure of the reaction centres, in the organisation of the photosystem and in the location of the electron transport components (Meunier *et al.*, 1998). The photochemical activity of PS II slowly decreases during the anaerobiosis period. In aerobic conditions, the PS II activity is quickly down-regulated, and the electron transfer from PS II to PS I decreases (Antal *et al.*, 2003).

The photochemical efficiency of PS II (F/F_m) was quite large in the control samples. In conditions of anaerobiosis, F/F_m increased in the first 40 min, then reduced significantly. A similar progression characterized the quantum yield of nonregulated energy (Y_{NO}) (Fig. 7). The effective PS II quantum yield (Y_{II}) decreased in the first 40 min of argon treatment, and reached the control level towards the end of the treatment.

The reaction centre PS II is optimized by the conversion of the light energy into a chemical stable energy: the transfer reactions are reversible and the separate state of the charges may be lost in the process of the charge recombination (Cser and Vass, 2007). Generally, the over-excitation of PS II is prevented by the antenna down-regulation, which removes the excess of energy as heat dissipation. This involves a series of processes named NPQ (non-photochemical quenching) and which are measured by the quenching of the chlorophyll fluorescence (Cruz *et al.*, 2005).

The coefficients of photochemical quenching, q_P and q_L , reached high values in conditions of anaerobiosis, compare with the control, values closed to 1 (Fig. 8). Thus, the oxidative state of the reaction centres was dominant. The q_P coefficient reflects the fraction of the opened reaction centres PS II in a "puddle" model of pigment organization, and q_L reflects the fraction of the opened reaction centres PS II in a "lake" model of pigment organization.

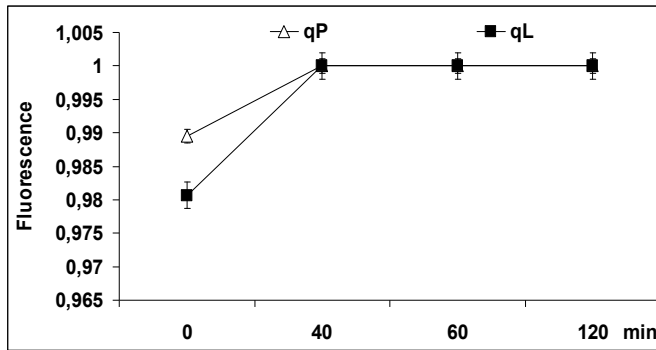


Fig. 8. The evolution of the coefficients of photochemical quenching qP and qL of PS II under argon treatment (120 min), compare with the control (0 min).

The fluorescence varies between F_0 , when a maximal quenching of photochemistry is reached and F_m , when Q_A accumulates in a reductive state. After F_m , the fluorescence decreases due to the NPQ (Cadoret *et al.*, 2004).

The fluorescence kinetics analyzed with the saturation pulse in control probes, highlighted the differences between the fluorescence parameters and the redox state (Fig. 9). The fluorescence induction curve, following the application of two saturation pulses, showed the differences between F_m and F'_m , based on the redox state of the components.

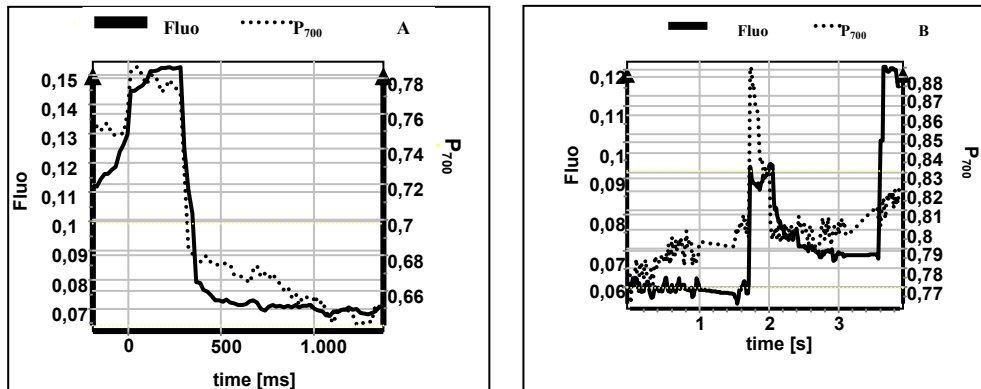


Fig. 9. The kinetics of the fluorescence induction with saturation pulse in *Cylindrospermum alatosporum* AICB 39 in control (A) and the induction curve (B); fluorescence of PS II (Fluo) and the activity of photosystem PS I (P_{700}).

In dark, the reaction centres of PS II are opened and prepared to absorb the light energy. O small quantity of light applied on the probe is enough to induce the minimal fluorescence of the chlorophyll (F_0). At a single saturation pulse, the reaction centres become closed (reduced) inducing the maximal fluorescence of the

chlorophyll (F_m). At the end of the anaerobiosis, the fluorescence induction showed balanced relations among the fluorescence parameters, and the induction curve followed a relatively normal progression (Fig. 10).

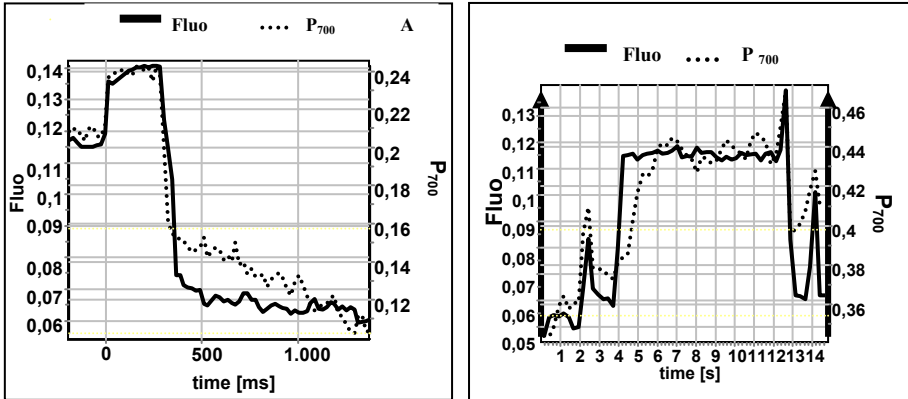


Fig. 10. The kinetics of the fluorescence induction with the saturation pulse in *Cylindrospermum alatosporum* AICB 39 at the end of the anaerobiosis conditions (A) and the induction curve (B); PS II fluorescence (Fluo) and the activity of the photosystem PS I (P700).

In the presence of DCMU inhibitor, F_0 and F_m presented the same relative values, and in conditions of anaerobiosis, they reduced significantly. This evolution determined the reducing of F_v which got negative values (Fig. 11). The photochemical efficiency of PS II (F/F_m), in the presence of DCMU, presented very high values, close to 1, both in control and in anaerobiosis, due to the opening of the reaction centres PS II. The effective PS II quantum yield (Y_{II}) decreased significantly, which showed that the energy of the absorbed photons is not use in photochemistry at the level of the reaction centres PS II. Also, the quantum yield of the nonregulated energy (Y_{NO}) showed high values, proving the inefficiency of the photochemical reactions at the level of the reaction centres.

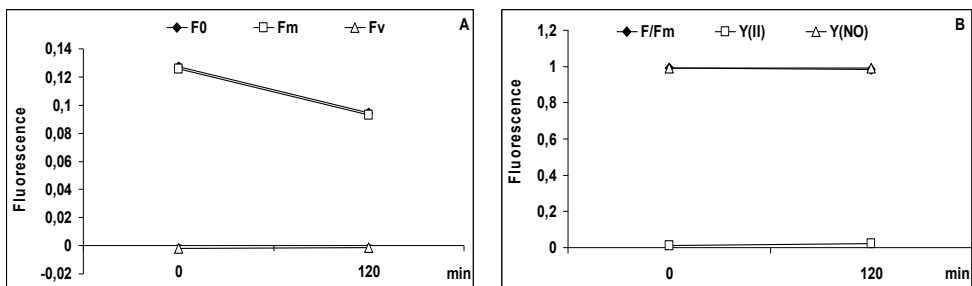


Fig. 11. The evolution of the fluorescence parameters of PS II (A) and the quantum yields (B) in control (0 min) and under argon treatment (120 min) in DCMU presence.

The coefficient of photochemical quenching, qP and qL , reached high values close to 1, attesting total closure of the reaction centres PS II, in DCMU presence (Fig. 12).

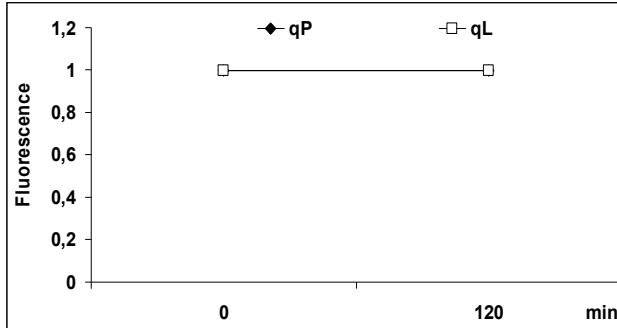


Fig. 12. The evolution of the coefficients of the photochemical quenching of PS II in control (0 min) and under argon treatment (120 min) in DCMU presence.

DCMU can block the transport of the electrons to PS II accepting side. It inhibits the quinone reduction from the Q_B side. The kinetics of the induction under DCMU influence is specific: the fluorescence reaches high values, from F_o to F_m , because Q_A is reduced through the photochemistry of the reaction centres and it is not oxidized through Q_B , which is blocked. In the DCMU presence, the fluorescence rate is dependent of the intensity of light and the functional state of the antenna PS II.

Conclusions

The results on the effect of the atmospheric gases with the induction of anaerobiosis concerning the activity of the photosystem PS II relate to the dynamics of the chlorophyll fluorescence and that of the photosynthetic components specific to each strain of cyanobacteria.

The activity of the photosystems PS II pointed out by the minimal fluorescence yield (F_o) and maximal fluorescence yield (F_m) reduced in the first 60 min of anaerobiosis, following a slightly increase at the end of the argon treatment. The redox state of oxidation/reduction of the reaction centres PS II decreased in intensity in the first moments of anaerobiosis.

The maximal PS II quantum yield (F/F_m) and the effective quantum yield (Y_{II}) recorded a high variability in relation with the species. The quantum yield of the nonregulated energy dissipation (Y_{NO}) was intense during the treatment. The photochemical coefficients qP and qL had a similar increase, and the values were close to one, depicting the oxidative state of the reaction centres PS II. The photochemical quenching and the quantum yield of the unregulated dissipation reached maximal values, which denote that a weak photochemical conversion of the energy exists at the level of the antenna complex for harvesting the light. The fluctuations of the oxidation/reduction are well highlighted through the kinetics of the fluorescence induction and by fluorescence curve.

In the presence of DCMU inhibitor (3-(3,4-dichlorophenyl)-1, 1-dimethylurea) which inhibits the electron transfer from the reaction centres PS II to plastoquinone, a weak state of energizing was recorded, leading to relatively equal values between F_o and F_m , because all the reaction centres PS II become closed (reduced), determining the decreasing of the variable fluorescence (F_v). DCMU is involved in the total closure of the reaction centres PS II.

Acknowledgements

This research was supported by POS-CCE Program nr. 236/16.08.2010.

REFERENCES

- Antal, T. K., Krendeleva, T. E., Laurinavichene, T. V., Makarova, V. V., Ghirardi, M. L., Rubin, A. B., Tsygankov, A. A., Seibert, M. (2003). The dependence of algal H_2 production on photosystem II and O_2 consumption activities in sulfur-deprived *Chlamydomonas reinhardtii* cell. *Biochim. Biophys. Acta*, **1607**, 153-160.
- Benemann, J. R. (2000). Hydrogen production by microalge. *J. Appl. Phycol.*, **12**, 291-300.
- Beutler, M., Wiltshire, K. H., Arp, M., Kruse, J., Reineke, C., Moldaenke, C., Hansen, U. P. (2003). A reduced model of the fluorescence from the cyanobacterial photosynthetic apparatus designed for the in situ detection of cyanobacteria. *Biochim. Biophys. Acta*, **1604**, 33-46.
- Cadoret, J. C., Demoulière, R., Lavaud, J., Gorkom, H. J., Houmard, J., Etienne, A. L. (2004). Dissipation of excess energy triggered by blue light in cyanobacteria with CP 43' (*isiA*). *Biochim. Biophys. Acta*, **1659**, 100-104.
- Cruz, J. A., Avenson, T. J., Kanazawa, A., Takizawa, K., Edwards, G. E., Kramer, D. M. (2005). Plasticity in light reactions of photosynthesis for energy production and photoprotection. *J. Exp. Bot.*, **56** (411), 395-406.
- Cser, K., Vass, I. (2007). Radiative and non-radiative charge recombination pathways in photosystem II studied by thermoluminescence and chlorophyll fluorescence in the cyanobacterium *Synechocystis* 6803. *Biochim. Biophys. Acta*, **1767**, 233-243.
- Grudziński, W., Krupa, Z., Garstka, M., Maksymiec, W., Swartz, T. E., Guszecki, W. I. (2002). Conformational rearrangement in light-harvesting complex II accompanying light-induced chlorophyll *a* fluorescence quenching. *Biochim. Biophys. Acta*, **1554**, 108-117.
- Karapetyan, N. V. (2007). Non-photochemical quenching of fluorescence in cyanobacteria. *Biochemistry (Moscow)*, **72** (10) 1127-1135.
- Krause, G. H., Weis, E. (1991). Chlorophyll fluorescence and photosynthesis: the basics. *Annu.Rev.Plant Physiol.Plant Mol.Biol.*, **42**, 313-349.
- Levin, D. B., Pitt, L., Love, M. (2004). Biohydrogen production: prospects and limitations to practical application. *Int. J. Hydrogen Energy.*, **29**, 173-185.

- Melis, A. (2007). Photosynthetic H₂ metabolism in *Chlamydomonas reinhardtii* (unicellular green algae). *Planta*, **226**, 1075-1086.
- Meunier, P. C., Coló-López, M. S., Sherman, L. A. (1998). Photosystem II cyclic heterogeneity and photoactivation in the diazotrophic, unicellular cyanobacterium *Cyanothece* species ATCC 511421. *Plant Physiol.*, **116**, 1551–1562.
- Prince, R. C., Ksheshgi, H. S. (2005). The photobiological production of hydrogen: potential efficiency and effectiveness as a renewable fuel. *Crit. Rev. Microbiol.*, **31**, 19-31.

A MATHEMATICAL MODELING FOR AN EPIDEMIC WITH RESPECT TO THE IMMIGRATION

MAHBOOBEH MOHAMADHASANI^{1,✉} and MASOUD HAVESHKI²

SUMMARY. In this paper we introduce a mathematical model for some contagious diseases which have temporary immunity with respect to the immigration. Then we get the equilibrium points for this model and distinguish the stability.

Key words: equilibrium point, Hamiltonian system, immigration, infective and immune people, SIRS Model, stability, susceptible people.

Introduction

Mathematical epidemiology has a long history going back to the smallpox model of Daniel Bernoulli in 1760. Much of the basic theory was developed between 1900 and 1935. In 1927, Kermack and McKendrick (Kermack and McKendrick, 1927) introduced a famous SIR epidemic model to study the law of the black plague. In 1932 an SIS Mathematical model was constructed and the threshold theory was established (Bailey, 1975). Many epidemic models are based on dividing the population into small numbers of compartments each containing individuals that are identified in terms of their status with respect to the disease in question (Capasso, 1993, Murray, 1989). Also we constructed a mathematical model of contagious diseases based on its properties and time (Mohamadhasani and Haveski, 2011).

Motivated by (Farkas, 2001, Mollison, 1984) , in this paper we establish an epidemic model based on temporary immunity, meaning the disease is contagious and people after recovery, get immunity, but the immunity is not for ever and ever. It is for a short time. Also, we assume that the newborn people are important. Some of them are maybe infective at time of birth. Natural death is important, too.

All the time there are some people who die but not because of considerable epidemic. The most important phenomena is immigration in this model. We pay attention to this reality which, there are some infective or susceptible or immune people who immigrate into the society. Also the immigrant group who leave the society are infective or susceptible or immune. This property is effective on the model. The last group in the model is dead people who die because of the epidemic.

¹ ✉ **Corresponding author**, Department of Mathematics, Hormozgan University, Bandarabas, Iran.
E-mail: ma.mohamadhasani@gmail.com

² Department of Mathematics, Hormozgan University, Bandarabas, Iran.
E-mail: ma.haveski@gmail.com

It is to be noted that in this model there is not latent period for the illness; A susceptible person who has contacted the disease becomes infective immediately. If incubation is short, this observation may be accepted. In this paper we introduce a model with respect to the immigration, natural death, birth speed, death because of disease, and this important property: temporary Immunity. At the end of section 2, we see the model is a part of a Hamiltonian system in dimensional 10. Then in section 3 and 4 we get equilibrium points and distinguish if they are stable or not.

SIRS Model

At first we consider the definition of susceptible, infective and immune people.

Susceptible: individuals who have no immunity to the infectious agent, so might become infected if exposed. The number of these people is denoted by $S(t)$ at time t .

Infective people: individuals who are currently infected and can transmit the infection to susceptible individuals who they contact. We denote the number of them by $I(t)$ at time t .

Immune people: Individuals who are immune to the infection and consequently do not affect the transmission dynamics in any way when they contact other individuals (Brauer, van der Driessche, and Wu, 2008). The number of Immune people are denoted by $R(t)$ at time t .

The fourth group in the society is the people who die because of epidemic. We show the number of this group by $D(t)$ at time t . There is a constant flow A of people who immigrate to the society. Also we assume constant fractions $p, q, (0 \leq p, q \leq 1)$. p and q display the percentages of infective and immune immigrant people who enter into the society, respectively. Then $1 - (p + q)$ is the percentage of immigrant people into the society who are susceptible. A is another constant flow of people who immigrate outside of society (leave the society) and p', q' are constant fractions, $(0 \leq p', q' \leq 1)$. p' and q' display the percentages of people who immigrate outside (leave) the society also are infective and immune, respectively.

Let there is a constant flow of new born people which is denoted by B . We pay attention to this reality that, there are maybe some infective newborn people which the percentage of this infective group is denoted by fraction u . Hence $1 - u$ is the percentage of susceptible newborn people. Let $d \geq 0$ is natural death rate in the society. This death is not related to the epidemic.

$r > 0$ is a positive quantity which called infective rate. $a > 0$ is another positive quantity which called Removed rate. This quantity distinguishes the rate of

entering people from Immune group into susceptible group. It is to be noted that immunity is temporary.

$b > 0$ is a positive quantity which called recovery rate. Finally, c is the last quantity which is called death rate because of epidemic. We pay attention to this reality that $c \geq 0$. Then the differential equations system for the epidemic is

$$\begin{aligned} \dot{S} &= -rSI + (1 - (p + q))A - dS + aR - (1 - (p' + q'))A' + (1 - u)B \\ \dot{I} &= rSI - bI - cI + uB - dI + pA - p'A' \\ \dot{R} &= bI - dR - aR + qA - q'A' \\ \dot{D} &= cI \end{aligned}$$

The initial conditions attached to the system is

$$S_0 = S(0) > 0, I_0 = I(0) > 0, \text{ and } R_0 = R(0) = 0$$

Usually, we assume that the disease starts with a small number of infectives. It means I_0 is small with respect to S_0 . We have an epidemic when the number of infective people is increasing faster than the number of people who recovers. The threshold parameter $\frac{b}{r}$ is called the relative recovery rate, which is the percentage of those recovered in unit time divided by the percentage of those infected by a single infective in unit time (Farkas, 2001). Also we have

$$R\left(t + \frac{1}{b}\right) - R(t) \cong \dot{R}(t) \frac{1}{b} = I(t) - \frac{d + a}{b}R(t) + \frac{q}{b}A - \frac{q'}{b}A'$$

Then

$$R\left(\frac{1}{b}\right) = I(0) + \frac{q}{b}A - \frac{q'}{b}A'$$

Similarly

$$D\left(\frac{1}{c}\right) = I(0)$$

Let U be the time in above model. Then we have the following five-dimensional system

$$\begin{aligned} \dot{S} &= -rSI + (1 - (p + q))A - dS + aR - (1 - (p' + q'))A' + (1 - u)B \\ \dot{I} &= rSI - bI - cI + uB - dI + pA - p'A' \\ \dot{R} &= bI - dR - aR + qA - q'A' \end{aligned}$$

$$\dot{D} = cI$$

$$\dot{U} = 1$$

This system is a part of a Hamiltonian system in dimensional 10. In fact the Hamiltonian function

$$\begin{aligned} H(S, I, R, D, U, V, X, W, Y, Z) \\ = -rSIV + (1 - (p + q))AV - dSV + aRV - (1 - (p' + q'))A'V + (1 - u)BV \\ + rSIX - bIX - cIX + uBX - dIX + pAX - p'A'X + bIW - (d + a)RW \\ + qAW - q'A'W + cIY + Z + g(S, I, R, D, U) \end{aligned}$$

where g is an arbitrary smooth function, creates the following 10-dimensional Hamiltonian system:

$$\dot{S} = -rSI + (1 - (p + q))A - dS + aR - (1 - (p' + q'))A' + (1 - u)B$$

$$\dot{I} = rSI - bI - cI + uB - dI + pA - p'A'$$

$$\dot{R} = bI - dR - aR + qA - q'A'$$

$$\dot{D} = cI$$

$$\dot{U} = 1$$

$$\dot{V} = rIV + dV - rIX - \frac{\partial g}{\partial S}$$

$$\dot{X} = rSV - rSX + bX + cX + dX - bW - cY - \frac{\partial g}{\partial I}$$

$$\dot{W} = -aV + (d + a)W - \frac{\partial g}{\partial R}$$

$$\dot{Y} = -\frac{\partial g}{\partial D}$$

$$\dot{Z} = -\frac{\partial g}{\partial U}$$

Equilibrium points

In this section we get the equilibrium points for this model.

By solving the following system we can have the equilibrium points.

$$-rSI + (1 - (p + q))A - dS + aR - (1 - (p' + q'))A' + (1 - u)B = 0 \quad (1)$$

$$rSI - bI - cI + uB - dI + pA - p'A' = 0 \quad (2)$$

$$bI - dR - aR + qA - q'A' = 0 \quad (3)$$

$$\dot{D} = cI = 0 \quad (4)$$

If $I(t) = 0$ then the epidemic is died. Then $I(t) \neq 0$ and by (4)

$$c = 0 \text{ or } D(t) = k, \text{ for all } t \in R^+, \text{ where } k \text{ is a constant.} \quad (5)$$

Then by (3) we have

$$R = \frac{qA - q'A' + bI}{d + a} \quad (6)$$

By (2) and (5) we have

$$S = \frac{p'A' - pA + bI + dI - uB}{rI}$$

By (1), (6) and (7) we have

$$-p'A' + pA - bI - dI + uB + (1 - (p + q))A - \frac{dp'A' - dpA + dbI + d^2I - duB}{rI} + \frac{aqA - aq'A' + abi}{d+a} + (1 - u)B - (1 - (p' + q'))A' = 0 \quad (8)$$

Hence

$$\begin{aligned} & \left(-br - dr + \frac{abr}{d+a} \right) I^2 \\ & + \left(-p'A'r + pAr + urB + (1 - (p + q))Ar - db - d^2 + \frac{aqA - aq'A'}{d+a} r \right. \\ & \left. + (1 - u)Br - (1 - (p' + q'))A'r \right) I + dpA - dp'A' + duB = 0 \end{aligned}$$

By the assumption $t_1 = -br - dr + \frac{abr}{d+a}$ and

$$t_2 = -p'A'r + pAr + urB + (1 - (p + q))Ar - db - d^2 + \frac{aqA - aq'A'}{d+a} r + (1 - u)Br - (1 - (p' + q'))A'r$$

and finally

$$t_3 = dpA + duB - dp'A' \text{ and } t_1 \neq 0 \text{ we have}$$

$$I = \frac{-t_2 + \sqrt{t_2^2 - 4t_1t_3}}{2t_1} \text{ and } I = \frac{-t_2 - \sqrt{t_2^2 - 4t_1t_3}}{2t_1}. \text{ Since } I(t) > 0 \text{ we have}$$

(1) If $t_2^2 - 4t_1t_3 > 0$ and $\frac{-t_2 - \sqrt{t_2^2 - 4t_1t_3}}{2t_1} > 0$ then $I(t) = \frac{-t_2 - \sqrt{t_2^2 - 4t_1t_3}}{2t_1}$.

(2) If $t_2^2 - 4t_1t_3 > 0$ and $\frac{-t_2 + \sqrt{t_2^2 - 4t_1t_3}}{2t_1} > 0$ then $I(t) = \frac{-t_2 + \sqrt{t_2^2 - 4t_1t_3}}{2t_1}$.

(3) If (1) and (2) are not correct then quadratic equation does not have any solution. Hence we do not have any equilibrium point.

$$\text{If } I = \frac{-t_2 + \sqrt{t_2^2 - 4t_1t_3}}{2t_1} > 0 \text{ or } I = \frac{-t_2 - \sqrt{t_2^2 - 4t_1t_3}}{2t_1} > 0 \text{ then}$$

$$((S(t), I(t), R(t), D(t))) =$$

$$\left(\frac{p'A' - pA + b \frac{-t_2 - \sqrt{t_2^2 - 4t_1t_3}}{2t_1} + d' \frac{-t_2 - \sqrt{t_2^2 - 4t_1t_3}}{2t_1} - \alpha B}{r \frac{-t_2 - \sqrt{t_2^2 - 4t_1t_3}}{2t_1}}, \frac{-t_2 - \sqrt{t_2^2 - 4t_1t_3}}{2t_1}, \frac{qA - q'A' + b \frac{-t_2 - \sqrt{t_2^2 - 4t_1t_3}}{2t_1}}{d + a}, k \right)$$

or

$$((S(t), I(t), R(t), D(t))) =$$

$$\left(\frac{p'A' - pA + b \frac{-t_2 + \sqrt{t_2^2 - 4t_1t_3}}{2t_1} + d' \frac{-t_2 + \sqrt{t_2^2 - 4t_1t_3}}{2t_1} - \alpha B}{r \frac{-t_2 + \sqrt{t_2^2 - 4t_1t_3}}{2t_1}}, \frac{-t_2 + \sqrt{t_2^2 - 4t_1t_3}}{2t_1}, \frac{qA - q'A' + b \frac{-t_2 + \sqrt{t_2^2 - 4t_1t_3}}{2t_1}}{d + a}, k \right)$$

is the equilibrium point, respectively.

We pay attention to this that if both of (1) and (2) are correct, then

$$((S(t), I(t), R(t), D(t))) =$$

$$\left(\frac{p'A' - pA + b \frac{-t_2 - \sqrt{t_2^2 - 4t_1t_3}}{2t_1} + d' \frac{-t_2 - \sqrt{t_2^2 - 4t_1t_3}}{2t_1} - \alpha B}{r \frac{-t_2 - \sqrt{t_2^2 - 4t_1t_3}}{2t_1}}, \frac{-t_2 - \sqrt{t_2^2 - 4t_1t_3}}{2t_1}, \frac{qA - q'A' + b \frac{-t_2 - \sqrt{t_2^2 - 4t_1t_3}}{2t_1}}{d + a}, k \right)$$

and

$$((S(t), I(t), R(t), D(t))) =$$

$$\left(\frac{p'A' - pA + b \frac{-t_2 + \sqrt{t_2^2 - 4t_1t_2}}{2t_1} + d \frac{-t_2 + \sqrt{t_2^2 - 4t_1t_2}}{2t_1} - uB}{r \frac{-t_2 + \sqrt{t_2^2 - 4t_1t_2}}{2t_1}}, \frac{-t_2 + \sqrt{t_2^2 - 4t_1t_2}}{2t_1}, \frac{qA - q'A' + b \frac{-t_2 + \sqrt{t_2^2 - 4t_1t_2}}{2t_1}}{d + a}, k \right)$$

are equilibrium points.

Stability

Now the next question to ask is if these equilibria are stable or not?

To provide an answer (Farkas, 2001) for this question we write out the Jacobi matrix of

$$N \times N \times N \times N \rightarrow N \times N \times N \times N$$

$$((S(t), I(t), R(t), D(t))) \rightarrow (-rSI + (1 - (p + q))A - dS + aR - (1 - (p' + q'))A' + (1 - u)B, rSI - bI - cI + uB - dI + pA - p'A', bI - dR - aR + qA - q'A', cI)$$

$$J = \begin{bmatrix} -rI - d & -rS & a & 0 \\ rI & rS - b - c - d & 0 & 0 \\ 0 & b & -d - a & 0 \\ 0 & c & 0 & 0 \end{bmatrix}$$

Then we get the eigenvalues of J .

$$\det(J - \lambda I) = \det \begin{bmatrix} -rI - d - \lambda & -rS & a & 0 \\ rI & rS - b - c - d - \lambda & 0 & 0 \\ 0 & b & -d - a - \lambda & 0 \\ 0 & c & 0 & \lambda \end{bmatrix} =$$

$$(-\lambda) \begin{vmatrix} -rI - d - \lambda & -rS & a \\ rI & rS - b - c - d - \lambda & 0 \\ 0 & b & -d - a - \lambda \end{vmatrix} =$$

$$\begin{aligned} & (-\lambda) (arIb - (d + a + \lambda)((-rI - d - \lambda)(rS - b - c - d - \lambda) + r^2SI)) = \\ & = (-\lambda)(arIb - (d + a + \lambda)(-r^2SI + rIb + rcl + rId + rI\lambda - drS + db + dc + d^2 + d\lambda - rS\lambda + b\lambda + c\lambda + d\lambda + \lambda^2 + r^2SI)) = (-\lambda)(arIb - (-r^2ISd - r^2ISa - r^2IS\lambda + rIbd + rIab + rIb\lambda + \end{aligned}$$

$$rcld + raci + rcl\lambda + rld^2 + radi + rld\lambda + rdl\lambda + ral\lambda + r\lambda^2 - d^2rS - darS - drS\lambda + d^2b + dab + db\lambda + d^2c + dac + dc\lambda + d^3 + d^2a + d^2\lambda + d^2\lambda + ad\lambda + d\lambda^2 - rdS\lambda - rS\lambda a - rS\lambda^2 + bd\lambda + ab\lambda + b\lambda^2 + cd\lambda + ac\lambda + c\lambda^2 + d^2\lambda + ad\lambda + d\lambda^2 + d\lambda^2 + a\lambda^2 + \lambda^3 + r^2SId + r^2SIa + r^2SI\lambda = (-\lambda)(-rldb - rlb\lambda - rcl d - raci - rcl\lambda - rld^2 - radi - 2rld\lambda - ral\lambda - r\lambda^2 + d^2rS + darS + 2drS\lambda - d^2b - abd - 2bd\lambda - d^2c - adc - 2cd\lambda - d^3 - d^2a - 2d^2\lambda - 2ad\lambda - d\lambda^2 + rS\lambda a + rS\lambda^2 - ab\lambda - b\lambda^2 - ac\lambda - c\lambda^2 - d^2\lambda - 2d\lambda^2 - a\lambda^2 - \lambda^3)$$

Then

$$P_n(\lambda) = (rldb - rcl d + raci + rld^2 + radi - d^2rS - darS + d^2b + abd + d^2c + adc + d^3 + d^2a)\lambda + (r\lambda b + rcl + 2rld + ral - 2drS + 2bd + 2cd + 2d^2 + 2ad - rSa + ab + ac + d^2)\lambda^2 + (r\lambda + d - rS + b + c + 2d + a)\lambda^3 + \lambda^4$$

and in

$$((S(t), I(t), R(t), D(t))) =$$

$$\left(\frac{p'A' - pA + b \frac{-t_2 - \sqrt{t_2^2 - 4t_1t_3}}{2t_1} + d \frac{-t_2 - \sqrt{t_2^2 - 4t_1t_3}}{2t_1} - uB}{r \frac{-t_2 - \sqrt{t_2^2 - 4t_1t_3}}{2t_1}}, \frac{-t_2 - \sqrt{t_2^2 - 4t_1t_3}}{2t_1}, \frac{qA - q'A' + b \frac{-t_2 - \sqrt{t_2^2 - 4t_1t_3}}{2t_1}}{d + a}, k \right)$$

and

$$((S(t), I(t), R(t), D(t))) =$$

$$\left(\frac{p'A' - pA + b \frac{-t_2 + \sqrt{t_2^2 - 4t_1t_3}}{2t_1} + d \frac{-t_2 + \sqrt{t_2^2 - 4t_1t_3}}{2t_1} - uB}{r \frac{-t_2 + \sqrt{t_2^2 - 4t_1t_3}}{2t_1}}, \frac{-t_2 + \sqrt{t_2^2 - 4t_1t_3}}{2t_1}, \frac{qA - q'A' + b \frac{-t_2 + \sqrt{t_2^2 - 4t_1t_3}}{2t_1}}{d + a}, k \right)$$

by the following Theorem $P_n(\lambda)$ given in canonical form is unstable.

Then equilibrium points are not stable.

Theorem (Willems, 1970)

The polynomial $P_n(\lambda) = \lambda^n + a_{n-1}\lambda^{n-1} + a_{n-2}\lambda^{n-2} + \dots + a_1\lambda + a_0$ is stable if and only if its coefficients are positive and all principal diagonal minors are positive in its Hurwitz matrix.

Conclusion

In this paper, a mathematical model of a contagious disease was introduced with respect to the important factors of it. Also we considered the equilibriums and their stability. A good point can be in what situations the system is periodic. Consideration of the model can be interesting for future researches.

REFERENCES

- Bailey, N. T. J. *The Mathematical Theory of Infectious Disease*, Hafner Press, New York., 1975.
- Brauer, F., van der Driessche, P. Wu, J. (Eds.). *Mathematical Epidemiology*, Series: Lecture Notes in Mathematics, Vol. **1945**, Springer-Verlag. 2008.
- Capasso, V. *Mathematical Structures of Epidemic Systems*, Series: Lecture Notes in Biomathematics vol. **97**, Springer-Verlag, 1993.
- Farkas, M. *Dynamical Models in Biology*, Academic Press, San Diego, 2001.
- Kermack, W. O., McKendrick, A. G. (1927). Contributions to the mathematical theory of epidemics, *Proc. R. Soc. Lond. A*, **115** (772), 700-721.
- Mollison, D. (1984). Simplifying simple epidemic models, *Nature*, **310**, 224-225.
- Murray, J. D. *Mathematical Biology*, Springer-Verlag, Berlin, 1989.
- Mohamadhasani, M., Haveski, M. (2011) A Mathematical Model for an Epidemic without Immunity. *Adv. Stud. Biol.*, **3** (1-4), 55-61.
- Willems, J. L. *Stability Theory of Dynamical Systems*, Wiley Interscience, New York, 1970.

EVALUATION OF THE INHIBITORY EFFECTS OF STATINS ON BLOOD VESSEL DEVELOPMENT - PROSPECTS FOR ANTIANGIOGENIC THERAPY OF CANCER

RAMONA MARIA MAXIM¹, MARIUS-COSTEL ALUPEI¹,
SEPTIMIU TRIPON² and MANUELA BANCIU^{3,✉}

SUMMARY. Statins have a primary activity related to cholesterol lowering in cardiovascular diseases. Besides their main pharmacological action, statins have pleiotropic activities with possible harmful effects on processes associated with tumor development: angiogenesis, inflammation, and metastasis.

The present work has shown the effects of statins on formation of blood vessels in a chicken chorioallantoic membrane (CAM) model *in vivo*. Statins have been selected based on their potency to reduce cholesterol levels in blood in the following order simvastatin > lovastatin > pravastatin. The inhibitory effects of statins on vasculature development might be a promise for their future application in anticancer antiangiogenic therapy.

Keywords: angiogenesis, CAM assay, statins

Introduction

Angiogenesis- the generation of new blood vessels from pre-existing vasculature is indispensable for physiological processes (*i.e.* wound healing) as well as for tumor growth and expansion (Folkman, 1972; Albini, *et al.*, 2005). In tumor angiogenesis, newly blood vessels formed from the vasculature of the healthy tissue surrounding the tumor, will provide a supply of nutrients and oxygen and prevent accumulation of metabolic waste products in tumors (Crowther *et al.*, 2001). After initiation of tumor angiogenesis, a key role in tumor blood vasculature formation is played by inflammatory cells such as T cells, monocytes, macrophages, neutrophils. The inflammatory cells infiltrating the tumor fully participate in the angiogenic process by recruitment, proliferation, migration and activation of the endothelial cells as well as by production of the majority of angiogenesis initiators. For that reason, this

¹ Faculty of Biology and Geology, Babes-Bolyai University, Cluj-Napoca, Romania.

² Electron Microscopy Center, Faculty of Biology and Geology, Babes-Bolyai University, Cluj-Napoca, Romania.

^{3,✉} **Corresponding author**, Department of Molecular Biology and Biotechnology, Faculty of Biology and Geology, Babes-Bolyai University, 400006/ Cluj-Napoca, Romania.
E-mail: manuela.banciu@ubbcluj.ro

step of angiogenesis is also called tumor inflammatory angiogenesis (Albini, *et al.*, 2005, Naldini and Carraro, 2005). Consequently, inflammation-dependent angiogenesis seems to be a central force in tumor growth and expansion, a concept supported by the observation that the use of **non-steroidal anti-inflammatory drugs** (NSAIDs) leads to angiogenesis inhibition (Clevers, 2006; Albini, *et al.*, 2005; Banciu *et al.*, 2008).

Although statins have a primary activity not related to angiogenesis, inflammation or tumor growth inhibition (*i.e.* cholesterol lowering in cardiovascular diseases) possess anti-inflammatory activity (Banciu, 2007; Coimbra M. *et al.*, 2010). Besides their primary pharmacological activity, several studies have shown pleiotropic effects of statins on cancer cells, *in vitro* as well as *in vivo* tumor models such as, anti-inflammatory, immunomodulatory and anti-angiogenic effects (Wong *et al.*, 2002; Jakobisiak and Golab, 2003; Graaf *et al.*, 2004). These effects are related to the reduced formation of isoprenoids via the inhibition of **3-hydroxy-3-methylglutaryl-coenzyme A (HMG-CoA) reductase**, the rate-limiting enzyme in hepatic cholesterol synthesis (Goldstein and Brown, 1990; Grundy, 1998). In turn, statins are responsible for post-translational modifications of signaling proteins including the small GTPases: Rac, Ras, and Rho (Coimbra *et al.*, 2010). These proteins, which were originally described as oncoproteins, have key player roles in intracellular inflammatory pathways involved in cell proliferation, differentiation, angiogenesis, and apoptosis (Demierre *et al.*, 2005; Hindler *et al.*, 2006; Greenwood, 2006). Several studies have shown that simvastatin inhibited angiogenesis in two experimental models, **vascular endothelial growth factor (VEGF)**–stimulated chick chorioallantoic membranes and **basic fibroblast growth factor (bFGF)**–stimulated mouse corneas (Park *et al.*, 2002). The anti-angiogenic activity of simvastatin was induced by inhibition of geranylgeranylation of RhoA and finally, membrane localization of RhoA, a protein involved in the mechanism of VEGF action (Park *et al.*, 2002). Moreover, it has been demonstrated that lovastatin enhanced response to chemotherapy in the B16 murine melanoma *in vivo* (Feleszko *et al.*, 1998; Feleszko *et al.*, 2002), induced apoptosis in melanoma cells (Shellman *et al.*, 2005; Collison *et al.*, 2002; Glynn *et al.*, 2008) and reduced the growth and angiogenesis in human melanoma cells, A375 and G361 as well as in the angiogenesis model *in vitro* obtained by co-culturing human dermal fibroblasts and human umbilical vein endothelial cells (HUVEC) (Depasquale and Wheatley, 2006).

Based on these previous findings, the aim of this research was to investigate whether statins might have strong inhibitory effects on formation of blood vessels in **chorioallantoic membrane (CAM)** of the chick embryo. To achieve this aim we have selected three types of statins based on their potency to reduce cholesterol levels in blood in the following order: simvastatin > lovastatin > pravastatin (Alberts *et al.*, 1980; Chao *et al.*, 1991; Masters *et al.*, 1995). The inhibitory effects of statins on angiogenesis might be a promise for further application in anticancer antiangiogenic therapy.

Materials and methods

***In vivo* angiogenesis model.** As *in vivo* angiogenesis model, the chorioallantoic membrane of the chick embryo was used and is termed in literature as CAM (chorioallantoic membrane) assay (Ribatti *et al.*, 1996; Ribatti, 2008; Tufan and Satiroglu-Tufan, 2005). CAM is widely used as *in vivo* angiogenic model because is a highly vascularized, respiratory tissue of the avian embryo, formed between days 4 and 5 of development. Moreover, it is easier to use and of limited ethical concern than other *in vivo* models. Moreover, it can be used as a model for inflammation (Zwadlo-Klarwasser *et al.*, 2001). To obtain the model fertilized hen eggs (*Gallus domesticus*) were incubated under constant humidified atmosphere, at 37 °C (Brooks *et al.*, 1999). All statin formulations were administered at day 7 after incubation of fertilized hen eggs by the opening in the shell under sterile conditions. At this time point angiogenesis as well inflammation are already developed in the experimental model (Zwadlo-Klarwasser *et al.*, 2001).

Quantification of statins. Determination of statin concentrations was performed by High Performance Liquid Chromatography (HPLC). We have extracted statins from commercially available products as following, Zeplan 40 mg (Gedeon Richter Romania S.A., Romania) for simvastatin; Medostatin 20 mg – (Medochemie Ltd, Cyprus) for lovastatin and Pravator 20 mg (Terapia Ranbaxy S.A., Romania) for pravastatin. All commercial formulations were homogenized. Statin extraction was performed in ethanol. Statins were quantified using a RP-18 column (5 µm) (Merck, Darmstadt, Germany), mobile phase: acetonitrile and water (35:65 (v/v %)), at pH 2 adjusted at with trifluoroacetic acid. Statins were determined by a UV detector, at 239 nm (Coimbra *et al.*, 2010). Statin stock concentrations determined by HPLC were: 0.9 mg/ml of simvastatin, 4.5 mg/ml of lovastatin, and 2.5 mg/ml of pravastatin.

Assessment of the effects of statins on CAM model. To study the effects of statins *in vivo*, different concentrations were placed via sterile filter paper disks (diameter of 0.5 cm) onto the surface of the growing CAM vessels at day 7 after incubation. For each type of statin, concentrations ranging from 2.2 to 50 µg/ml were tested. To obtain working concentrations of statins, stock concentrations prepared in ethanol, were diluted with Phosphate Buffered Saline (PBS). Ethanol toxicity was also tested. Untreated fertilized eggs were used as controls. Each experimental group consists of 5 eggs. At day 5 after incubation with statins, the effects of different concentrations of statins on the formation of the embryonic blood vessels and infiltration of inflammatory cells (heterofils, monocytes, lymphocytes) in the vicinity of the newly blood vessels were evaluated by macroscopic and microscopic observations. To visualize inflammatory infiltrate, May Grünwald -Giemsa stain was performed as described previously (Dacie and Lewis, 1995).

Statistical analysis. Data were presented as means±standard deviations of 5 individual counts. The differences between the effects of different treatments on blood vessel production were analyzed by one-way ANOVA with Dunnett's test for multiple comparisons using GraphPad Prism version 4.02 for Windows, GraphPad Software (San Diego, CA, U.S.A.). A value of $P<0.05$ was considered significant.

Results and discussions

To evaluate the **antiangiogenic effects of statins on blood vessel development in the chick embryos**, different statin concentrations ranging from 2.2 to 50 µg/ml were used. Statin selection was performed based on their potency to reduce cholesterol levels in blood in the following order simvastatin> lovastatin> pravastatin (Alberts *et al.*, 1980; Chao *et al.*, 1991; Masters *et al.*, 1995).). Antiangiogenic effects were assessed at day 5 after CAM incubations with statins. As stock solutions, all statins were prepared in ethanol, the toxicity of the solvent being also tested. Only a slight ethanol toxicity on blood vessel development was noted at the highest concentration of ethanol used for preparation of 50 µg/ml of statins (Table 1, Fig. 1, Panels A and B).

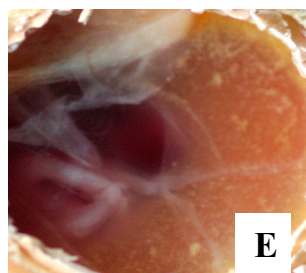
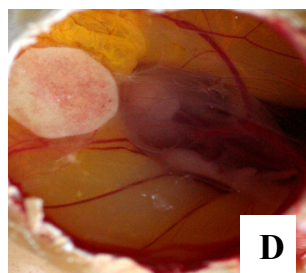
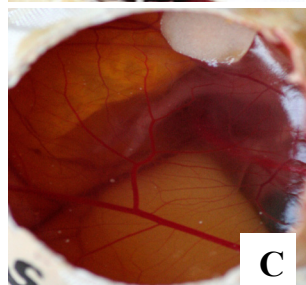
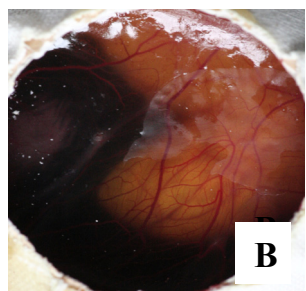
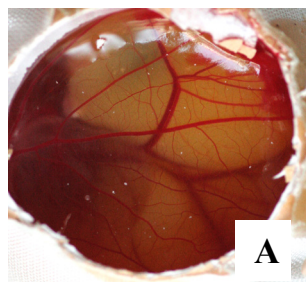
Table 1.

The antiangiogenic effects of statins on chick chorioallantoic membranes at the lowest concentration tested.

Experimental group	Number of large blood vessels	Number of small blood vessels	Observations
Control	6.8±0.8	34.6±8.8	
Ethanol	6.2±1.8	30.8±14.9	
SIM	5±1.2	12.4±1.1	Presence of hemorrhagic area
LOV	2.6±1.2	7.6±1.5	2 out of 5 eggs with necrosis area
PRV	1	-	4 out of 5 eggs with necrotic area

Abbreviations: SIM: simvastatin; LOV: lovastatin; PRV: pravastatin.

Data are presented as mean ± standard deviation. Effects of 2.2 µg/ml of each statin are shown.



At concentrations ranging from 5-50 $\mu\text{g/ml}$ all types of statins entirely inhibited development of blood vessels (not shown data).

We have shown only the effects at the lowest concentration tested at which we could clearly note the differences between different types of statins (Fig.1, Panels C, D, E and Table 1).

At 2.2 $\mu\text{g/ml}$, evaluation of CAM clearly showed a strong inhibition of number of large blood vessels (with diameter higher than 40 μm) after treatment with lovastatin (by 60%) and pravastatin (by 90%) compared to the controls (Tables 1 and 2). At the same concentration, simvastatin inhibited slightly development of large blood vessels but not statistically significant compared to the controls (Table 2).

By measuring and counting the thickness and number of vessels it was found that the number of blood vessel smaller than 40 μm was significantly changed by lovastatin and simvastatin by 60-80% compared to those developed in untreated embryos. No secondary blood vessel was noted after treatment with pravastatin also at the lowest concentration tested (Tables 1 and 2). Moreover lovastatin and pravastatin induced large areas of necrosis in CAM models. In addition to antiangiogenic actions exerted by statins, the analysis of inflammatory infiltrate has shown only rare lymphocytes after all statin treatments. No heterofils and monocytes were noted (data not shown). These findings might suggest that antiangiogenic effects exerted by statins on CAM model could be induced via the inhibition of the inflammation associated with angiogenesis.

Fig.1. Antiangiogenic effects of statin treatment in CAM model.

Panel A. Control = Untreated CAM;
 Panel B. Ethanol-treated CAM;
 Panel C. CAM treated with 2.2 $\mu\text{g/ml}$ of simvastatin;
 Panel D. CAM treated with 2.2 $\mu\text{g/ml}$ of lovastatin;
 Panel E. CAM treated with 2.2 $\mu\text{g/ml}$ of pravastatin.

Table 2.**Comparison between antiangiogenic effects of statins in CAM model.**

Comparison between experimental groups	Statistical significance
Control vs Ethanol	<i>ns</i>
Control vs SIM	<i>ns</i>
Control vs LOV	*
Control vs PRV	*
Ethanol vs SIM	<i>ns</i>
Ethanol vs LOV	<i>ns</i>
Ethanol vs PRV	*
SIM vs LOV	<i>ns</i>
SIM vs PRV	<i>ns</i>
LOV vs PRV	<i>ns</i>

Abbreviations: SIM: simvastatin; LOV: lovastatin; PRV: pravastatin.
Effects of 2.2 µg/ml of each statin are shown. P values are indicated as follows: *ns*, not significant ($P>0.05$); *, $P<0.05$.

Conclusions and discussions

In conclusion our data showed that selected statins differ in their ability to inhibit angiogenesis in this *in vivo* model. The highest antiangiogenic activity was induced after CAM incubation with pravastatin although pravastatin has the lowest potency to reduce cholesterol levels in blood. These effects might suggest that probably the effects of statins on blood vessel formation are not related to their reduced formation of isoprenoids via the inhibition of hepatic cholesterol biosynthesis (Goldstein and Brown, 1990; Grundy, 1998). It has already been shown that in primates pravastatin increased the activity of endothelial cells to produce NO without the reduction of LDL cholesterol levels (Laufs *et al.*, 1998; Stancu and Sima, 2001). Moreover, pravastatin in Pravator is administered as active compound while lovastatin and simvastatin are administered as inactive forms (lactones). Both formulations have to be enzymatically hydrolyzed to generate active forms of these statins (Laufs *et al.*, 1998; Stancu and Sima, 2001; Blumenthal, 2000).

Overall, our data offer preliminary evidence about antiangiogenic effects of statins in CAM model, which might be exploited in future *in vivo* experiments on inhibition of tumor angiogenesis/inflammation.

Acknowledgement

This work was supported by CNCS-UEFISCDI, project number PN II-RU PD- 387/2010.

REFERENCES

- Alberts, A.W., Chen J., Kuron, G., Hunt, V., Huff, J., Hoffman, C., Rothrock, J., Lopez, M., Joshua, H., Harris, E., Patchett, A., Monaghan, R., Currie, S., Stapley, E., Albers-Schonberg, G., Hensens, O., Hirshfield, J., Hoogsteen, K., Liesch, J., Springer J. (1980) Mevinolin: A highly potent competitive inhibitor of hydroxymethylglutaryl-coenzyme A reductase and a cholesterol-lowering agent. *Proc. Natl. Acad. Sci.* **77** (7): 3957-3961.
- Albini, A., Tosetti, F., Benelli, R., Noonan, D.M. (2005) Tumor inflammatory angiogenesis and its chemoprevention. *Cancer Res.*, **65**, 10637-10641.
- Banciu, M. (2007) *Liposomal Targeting of Glucocorticoids to Inhibit Tumor Angiogenesis*, PrintPartners Ipskamp, Enschede, pp 17.
- Banciu, M., Metselaar, J.M., Schiffelers, R.M., Storm, G., (2008) Antitumor activity of liposomal prednisolone phosphate depends on the presence of functional tumor-associated macrophages in tumor tissue. *Neoplasia*, **10** (2), 108-117.
- Blumenthal, R.S. (2000). Statins: Effective antiatherosclerotic therapy, *Am. Heart. J.*, **139**: 577-583.
- Brooks, P.C., Montgomery, A.M., Cheresch, D. A. (1999) Use of the 10-day-old chick embryo model for studying angiogenesis. *Methods Mol Biol.*, **129**, 257-269.
- Chao, Y, Chen, J. S., Hunt, V.M., Kuron, G.W., Karkas, J.D., Liou, R., Alberts, A.W. (1991) Lowering of plasma cholesterol levels in animals by lovastatin and simvastatin. *Eur J. Clin. Pharmacol.*, **40**, Suppl 1, S11-4.
- Clevers, H. (2006) Colon Cancer — Understanding How NSAIDs Work. *N. Engl. J. Med.*, **354**, 761-763.
- Coimbra, M., Banciu, M., Fens, M.H.A.M., de Smet, L., Cabaj, M., Metselaar, J.M., Storm, G., Schiffelers, R.M. (2010) Liposomal pravastatin inhibits tumor growth by targeting cancer-related inflammation *J. Control. Release*, **148** (3), 303-310.
- Collisson, E.A., Carranza, D.C., Chen, I.Y., Kolodney, M.S. (2002) Isoprenylation is necessary for the full invasive potential of RhoA overexpression in human melanoma cells. *J. Invest. Dermatol.*, **119**, 1172–1176.
- Crowther, M., Brown, N.J., Bishop, E.T., Lewis, C.E. (2001) Microenvironmental influence on macrophage regulation of angiogenesis in wounds and malignant tumors. *J. Leukoc. Biol.*, **70**, 478-490.
- Demierre, M.F., Higgins, P.D., Gruber, S.B., Hawk, E., Lippman, S.M. (2005) Statins and cancer prevention. *Nat. Rev. Cancer*, **5**, 930–942.
- Depasquale, I, Wheatley, D.N. (2006) Action of Lovastatin (Mevinolin) on an in vitro model of angiogenesis and its co-culture with malignant melanoma cell lines. *Cancer Cell. Int.*, **6**:9.
- Dacie, J., Lewis, S., *Practical haematology*. Churchill Livingstone, London, 1995.
- Feleszko, W., Zagodzón, R., Golab, J., Jakobsiak, M. (1998) Potentiated antitumour effects of cisplatin and lovastatin against MmB16 melanoma in mice. *Eur. J. Cancer*, **34**, 406-411.

- Feleszko, W., Mlynarczuk, I., Olszewska, D., Jalili, A., Grzela, T., Lasek, W., Hoser, G., Korczak-Kowalska, G., Jakobisiak, M. (2002) Lovastatin potentiates antitumor activity of doxorubicin in murine melanoma via an apoptosis-dependent mechanism. *Int. J. Cancer*, **100**, 111-118.
- Folkman, J. (1972) Anti-angiogenesis: a new concept for therapy of solid tumours. *Ann Surg.*, **175**, 409-416.
- Glynn, S.A., O'Sullivan, D., Eustace, A.J., Clynes, M., O'Donovan, N. (2008) The 3-hydroxy-3-methylglutaryl-coenzyme A reductase inhibitors, simvastatin, lovastatin and mevastatin inhibit proliferation and invasion of melanoma cells, *BMC Cancer*, **8**, 9.
- Goldstein, J.L., Brown, M.S. (1990) Regulation of the mevalonate pathway. *Nature*, **343**, 425-430.
- Graaf, M.R., Richel, D.J., van Noorden, C.J., Guchelaar, H.J. (2004) Effects of statins and farnesyltransferase inhibitors on the development and progression of cancer. *Cancer Treat. Rev.*, **30**, 609-641.
- Greenwood, J., Steinman, L., Zamvil, S.S. (2006) Statin therapy and autoimmune disease: from protein prenylation to immunomodulation. *Nat. Rev. Immunol.*, **6** (5), 358-370.
- Grundy, S.M. (1998) Statin trials and goals of cholesterol-lowering therapy, *Circulation*, **97**, 1436-1439.
- Hindler, K., Cleeland, C.S., Rivera, E., Collard, C.D. (2006). The role of statins in cancer therapy. *Oncologist*, **11**, 306-315.
- Jakobisiak, M., Golab, J. (2003). Potential antitumor effects of statins (Review). *Int. J. Oncol.*, **23**, 1055-1069.
- Laufs, U., Fata, V.L., Plutzky, J., Liao, J.K. (1998) Upregulation of endothelial nitric oxide synthase by HMG-CoA reductase inhibitors. *Circulation*, **97**, 1129-1135,
- Masters, B.A., Palmoski, M.J., Flint, O.P., Gregg, R.E., Wang-Iverson, D., Durham, S.K. (1995) *In vitro* myotoxicity of the 3-hydroxy-3-methylglutaryl coenzyme A reductase inhibitors, pravastatin, lovastatin and simvastatin, using neonatal rat skeletal myocytes. *Toxicol. Appl. Pharmacol.*, **131** (1), 163-174.
- Naldini, A., Carraro, F. (2005) Role of inflammatory mediators in angiogenesis, *Curr Drug Targets Inflamm. Allergy*, **4** (1), 3-8.
- Park, H.J., Kong, D., Iruela-Arispe, L., Begley, U., Tang, D., Galper, J.B. (2002) 3-Hydroxy-3-Methylglutaryl Coenzyme A Reductase Inhibitors Interfere With Angiogenesis by Inhibiting the Geranylgeranylation of RhoA. *Circ Res.*, **91**, 143-150.
- Ribatti, D., Vacca, A., Roncali, L., Dammacco, F. (1996) The chick embryo chorioallantoic membrane as a model for *in vivo* research on angiogenesis. *Int J Dev Biol.*, **40**, 1189-1197.
- Ribatti, D. (2008) The chick embryo chorioallantoic membrane in the study of tumor angiogenesis. *Romanian J. Morphol. Embryol.*, **49** (2), 131-135.
- Shellman, Y.G., Ribble, D., Miller, L., Gendall, J., Vanbuskirk, K., Kelly, D., Norris, D.A., Dellavalle, R.P. (2005) Lovastatin-induced apoptosis in human melanoma cell lines. *Melanoma Res.*, **15**, 83-89.

ANTIANGIOGENIC EFFECTS OF STATINS

- Stancu, C., Sima, A. (2001) Statins, mechanism of action and effects. *J. Cell. Mol. Med.*, **5** (4), 378-387.
- Tufan, A. C., Satiroglu-Tufan, N.L. (2005) The chick embryo chorioallantoic membrane as a model system for the study of tumor angiogenesis, invasion and development of anti-angiogenic agents. *Curr. Cancer Drug Targets*, **5** (4), 249-266.
- Wong, W.W., Dimitroulakos, J., Minden, M.D., Penn, L.Z. (2002) HMG-CoA reductase inhibitors and the malignant cell, the statin family of drugs as triggers of tumor-specific apoptosis. *Leukemia*, **16**, 508–519.
- Zwadlo-Klarwasser, G., Gorlitz, K., Hafemann, B., Klee, D., Klosterhalfen, B. (2001) The chorioallantoic membrane of the chick embryo as a simple model for the study of the angiogenic and inflammatory response to biomaterials. *J. Mater. Sci. Mater. Med.*, **12**, 195-199.

MYELOPEROXIDASE BUT NOT SUPEROXIDE DISMUTASE HAS A PROTECTIVE EFFECT IN THE *EX VIVO* MODEL OF BULLOUS PEMPHIGOID

EMILIA LICĂRETE^{1,2,✉}, CASSIAN SITARU^{1,3} and
MIRCEA TEODOR CHIRIAC²

SUMMARY. Bullous pemphigoid is an autoimmune blistering disease characterized by the presence of circulating and tissue-bound autoantibodies against two structural proteins of the hemidesmosomes, namely the bullous pemphigoid antigen of 180kDa and bullous pemphigoid antigen of 230kDa, respectively. The implication of immune players in the clinical outcome has been addressed in different studies over the past three decades and has led to the formulation of a general hypothesis that tried to explain the pathogenesis of the disease. According to this scenario, binding of autoantibodies to their target autoantigens is followed by the recruitment and activation of the complement system and further reinforced by the activation of granulocytes which release reactive oxygen species and subsequently activate proteases culminating in the enzymatic digestion of the dermal-epidermal zone. Despite our understanding in these general terms, the fine molecular processes underlying different steps of this scenario and their implications for a future targeted-therapy have yet to be ascertained. In the present study we investigated the potential of different modulators of reactive oxygen species production to induce or block tissue damage using the *ex vivo* model for bullous pemphigoid. Our present data indicate that despite its powerful scavenging effect of more than 85%, superoxide dismutase is not able to inhibit the blister-inducing capacity of autoantibodies. In contrast, specific inhibition of the myeloperoxidase could block the antibody-induced granulocyte-mediated dermal-epidermal separation. These results contribute to the further characterization of the pathogenic relevance of granulocytes in experimental bullous pemphigoid and should facilitate further investigations of the molecular pathogenesis of this and related diseases.

Non-standard abbreviations: AHAB, 4-aminobenzoic acid hydrazide; BP, bullous pemphigoid; DES, dermal-epidermal separation; IF, immunofluorescence; MPO, myeloperoxidase; PMA, phorbol 12-myristate 13-acetate; ROS, reactive oxygen species; SOD, superoxide dismutase.

Key words: autoimmunity, collagen XVII/BP180, myeloperoxidase, superoxide dismutase, tissue damage

¹ Department of Dermatology, University of Freiburg, Hauptstr. 7, 79104 Germany.

² Department of Experimental Biology and the Molecular Biology Center at the Institute for Interdisciplinary Research on Bio-Nano-Sciences, Babes-Bolyai University Cluj-Napoca, Romania.

³ Centre for Biological Signalling Studies (BIOS), University of Freiburg, Germany.

✉ **Corresponding author: Emilia Licărete**, Institute for Interdisciplinary Research on Bio-Nano-Sciences, 42 August Treboniu Laurian Street, 400271 Cluj-Napoca, Tel.: +4-(0)264-454554.
E-mail: emilia_licarete@yahoo.com

Introduction

Bullous pemphigoid (BP) is a chronic subepidermal blistering disease affecting elderly although a few childhood cases were reported. Circulating and tissue bound antibodies against two hemidesmosomal proteins namely BP230 and BP180 can be detected in BP patients (Yancey, 2005; Mihai & Sitaru, 2007). Clinically, patients present with tense blisters and erosions localized on either inflamed or non-inflamed skin and on the oral mucosa which can leave scars upon healing. Immunopathologically, linear IgG and/or complement component C3 deposits may be observed by direct immunofluorescence (IF) of perilesional skin whereas circulating auto-antibodies may be detected by indirect IF using the normal human skin as a substrate or by an ELISA with recombinant BP180. The histological examination of lesional skin reveals subepidermal blisters with an inflammatory infiltrate rich in eosinophils and neutrophils. Ultrastructurally, subepidermal split occurs at the level of lamina lucida of the basal membrane (Dvorak *et al.*, 1982; Olasz *et al.*, 2008; Sitaru, 2009).

The first evidence that BP autoantibodies are pathogenic comes from an *ex vivo* model developed by Gammon and co-workers (Gammon *et al.*, 1981) who demonstrated that the antibody-induced dermal epidermal separation (DES) was dependent upon the complement-dependent recruitment of leukocytes at the dermal-epidermal junction (Gammon *et al.*, 1981; Gammon *et al.*, 1982). Using a similar experimental setting, Sitaru and coworkers demonstrated that BP sera immuno-adsorbed against recombinant BP180 NC16A lose their capacity to induce DES suggesting that the immunodominant epitopes in BP180 may reside within its NC16A domain (Sitaru *et al.*, 2002b).

In 1993, Liu *et al.* demonstrated the pathogenicity of BP 180 autoantibodies *in vivo*. Passive transfer of rabbit IgG specific to the murine BP180 into neonatal mice induced clinical, histological, and immuno-pathological alterations similar to those observed in patients with BP (Liu *et al.*, 1993). Using this model, it has been shown in turn that activation of the classical pathway of complement, neutrophils, mast cells and macrophages are essential for the experimental induction of BP (Liu *et al.*, 1995; Liu *et al.*, 2000; Chen *et al.*, 2002; Chen *et al.*, 2001; Nelson *et al.*, 2006). Complement activation via the classical pathway triggered by anti-mBP180 immune complexes results in the generation of C5a, which is essential for neutrophil recruitment to the cutaneous basal membrane zone and for the subsequent DES. C5-deficient mice injected intra-dermally with a neutrophil chemoattractant, either C5a or IL-8, became susceptible to the pathogenic effects of anti-mBP180 IgG (Lessey *et al.*, 2008). F(ab')₂ fragments generated by digestion of pathogenic anti-mBP180 antibodies did not induce blistering in C5 sufficient mice demonstrating that complement activation is triggered by the Fc portion of the antibodies (Liu *et al.*, 1995).

In autoimmune blistering diseases, granulocytes have a crucial role in autoantibody mediated tissue damage. Experimental data supporting the involvement of granulocytes in blister formation comes from the *ex vivo* as well as *in vivo* models of blistering diseases. The antibody-induced DES requires the addition of granulocytes in the *ex vivo* models of bullous pemphigoid and the related disease epidermolysis bullosa acquisita.

Moreover, antibodies pathogenicity depends on their ability to activate Fc receptors on the surface of granulocytes (Sitaru *et al.*, 2002a; Sitaru *et al.*, 2002b).

The involvement of the reactive oxygen species (ROS) generated by the antibodies-activated neutrophils in autoimmune diseases is still controversial. In the experimental models of different autoimmune conditions, inhibition of the granulocytes ROS resulted in a reduced (van der Veen *et al.*, 2000; Ross *et al.*, 2004) or augmented severity of the disease (Hultqvist *et al.*, 2004). In the passive transfer model of epidermolysis bullosa acquisita it has been shown that the diseases development is dependent on the presence of functional nicotinamide adenine dinucleotide phosphate (NADPH) oxidase (Chiriac *et al.*, 2007).

The aim of the present study was to investigate the effect of exogenous bovine superoxide dismutase (SOD) and myeloperoxidase (MPO) inhibition in the *ex vivo* DES induced by bullous pemphigoid pathogenic antibodies. We showed that SOD could not limit the split formation in the skin incubated with pathogenic antibodies despite an important reduction of the superoxide amount as demonstrated by the luminol assay. However, specific MPO inhibition resulted in a reduction of blister-inducing capacity of antibodies. Our present data provide further evidence for the implication of ROS in the pathogenesis of BP. Nevertheless, ROS may be regarded as key players in autoimmunity with possible therapeutic implications.

Materials and Methods

Human sera

Serum samples were obtained from patients with bullous pemphigoid before the initiation of treatment as well as from healthy donors. BP patients were characterized by: (a) subepidermal skin blisters, (b) linear IgG deposits along the dermal-epidermal junction detected by direct IF microscopy, and (c) circulating IgG autoantibodies binding to the epidermal of the salt-split skin for BP as revealed by indirect IF microscopy/ELISA. The study was approved by the Ethics Committee of the Medical Faculty of the University of Freiburg, Germany (Institutional Board Projects no 318/07, 425/08, and 278/11). We obtained informed consent from patients whose material was used in the study, in adherence to the Helsinki Principles.

Indirect immunofluorescence

Circulating autoantibodies in BP sera were detected by indirect immunofluorescence following published protocols (Csorba *et al.*, 2010). Briefly, frozen sections from healthy human skin were incubated in a first step with a 5-fold diluted serum sample. The bound autoantibodies were then visualized using 100-fold diluted Alexa Fluor488-labeled polyclonal goat anti-human IgG antibody (Invitrogen).

Isolation of peripheral blood cells from healthy donors

Leukocytes were isolated by dextran sedimentation as previously described (Sitaru *et al.*, 2002b). Briefly, fresh peripheral blood from healthy donors was mixed 1:1 with 3 % dextran (Roth) prepared in 0.9 % NaCl and erythrocytes were allowed to sediment for 30 minutes. The remaining erythrocytes were subjected to hypotonic lysis with a 0.2 % NaCl solution. Leukocytes were washed with cell culture medium (Lonza) and adjusted to 3×10^7 cells/ml. Cells' viability was tested with trypan blue and cell suspensions with viability >95 % were further used in the study.

Ex vivo induction of dermal - epidermal separation by pathogenic antibodies

We used an *ex vivo* model for bullous pemphigoid following previously published protocols (Sitaru *et al.*, 2002b). Briefly, BP and control sera diluted 5-fold were incubated for 2 hours with human skin cryosections in a humid chamber, at room temperature. After washing with phosphate buffered saline sections were incubated with 500 μ l leukocytes suspension in cell culture medium for additional 3 hours at 37°C in a humidified incubator with 5 % CO₂. Finally slides were fixed in buffered formalin, stained with hematoxylin and eosin and scored by two investigators. To address the role of the SOD on the antibody induced DES, 1500 U/ml of bovine SOD (Sigma) was added to the leukocyte suspension. Furthermore, myeloperoxidase inhibition was achieved by the addition of 100 μ M 4-aminobenzoic acid hydrazide (ABAH) (Sigma) (Kettle *et al.*, 1997; Arvadia *et al.*, 2011) to the leukocytes before the incubation with the cryosections.

Evaluation of exogenous SOD activity in granulocytes stimulated with phorbol 12-myristate 13-acetate (PMA)

To assess the capacity of SOD to scavenge the superoxide anion produced by PMA-activated granulocytes, 1×10^6 cells were incubated in 96-well plates and mixed with 150 μ M luminol (Sigma) and 1500 U/ml SOD (Caldefie-Chézet *et al.*, 2002). Controls without SOD were also prepared. Luminescence was monitored every other minute for 30 minutes in an automated spectrophotometer (Sirius HT-TRF, MWG) at 37°C with intercalated shaking.

Results and discussions

BP serum autoantibodies bound at the dermal-epidermal junction

To test the ability of our bullous pemphigoid serum autoantibodies to recognize the antigen *in situ* we incubated normal skin sections with 5-fold diluted BP sera or healthy donor's sera as negative controls. After 30 minutes of incubation antibodies bound at the dermal epidermal junction could be visualized (Figure 1b) using 100-fold

diluted, Alexa Fluor488-labelled polyclonal goat anti-human IgG antibody. Antibodies from normal human serum didn't stain the skin basement membrane (Figure 1a). Since the initial step in the pathogenetic chain of events leading to the BP-associated tissue destruction is represented by the binding of autoantibodies to their target proteins we first evaluated the capacity of our BP sera to bind their specific antigens. As expected, in contrast to the antibodies in the serum of healthy individuals, the autoantibodies from BP patients stained the basal membrane in a specific pattern.

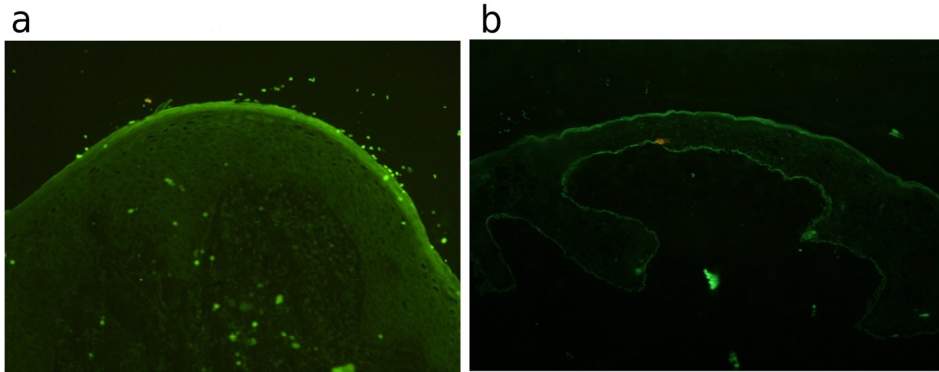


Figure 1. Autoantibodies from BP patients recognize their target antigens as revealed by indirect immunofluorescence. In contrast to the incubation of normal human sections with (a) normal human serum from a healthy donor that didn't stain the basement membrane, the incubation with (b) pathogenic BP serum resulted in a characteristic linear staining pattern.

Despite strong scavenging activity, SOD is not able to abolish the dermal-epidermal separation induced by BP autoantibodies

In another set of experiments, we aimed to investigate the effects of the addition of exogenous bovine SOD on the DES induced by bullous pemphigoid pathogenic antibodies. Therefore we incubated healthy human skin cryosections with antibodies from BP patients and normal human serum, respectively. After 2 hours of incubation at room temperature slides were washed and subsequently incubated with up to 500 μ l from a purified granulocyte suspension at a density of 3×10^7 cells/ml. For the slides incubated with SOD, granulocyte suspensions were supplemented with 1500 U/ml SOD. At the end of the incubation time, sections were washed several times and stained with hematoxylin and eosin. DES was observed in both untreated and SOD-treated sections which were incubated with BP serum (Figure 2a and b). No DES (Figure 2c) has been seen in sections incubated with control serum and with SOD or control serum without SOD, respectively (not shown). To study the pathogenic mechanisms responsible for blister formation in bullous pemphigoid several *ex vivo* and animal models have been developed so far (Gammon *et al.*, 1982; Liu *et al.*, 1993; Sitaru *et al.*, 2002b; Nishie *et al.*, 2007; Nishie *et al.*, 2009).

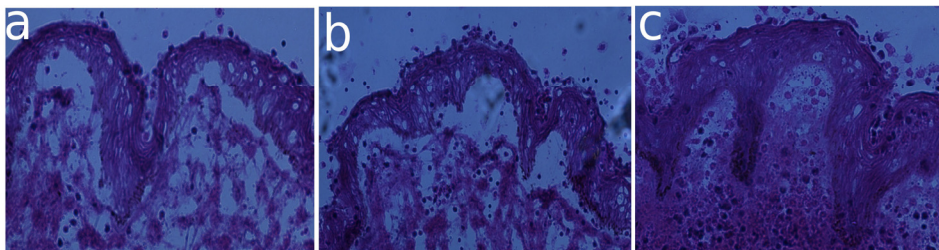


Figure 2. SOD does not inhibit the ability of BP autoantibodies to induce subepidermal splits *ex vivo*. (a) Subsequent addition of normal human leukocytes to human skin cryosections previously incubated with BP autoantibodies resulted in dermal-epidermal separation. (b) Addition of SOD to the purified granulocytes prior to their incubation with the cryosections did not limit the split formation capacity of BP autoantibodies. As expected, (c) normal human serum co-incubated with granulocytes did not induce split formation in cryosections.

Despite great advances in our understanding of the pathogenesis of BP many of the fine molecular mechanisms, e.g. the role of granulocyte-derived ROS, still remain obscure. In the present study we set out to explore the implications of superoxide and other ROS in the autoantibody-induced tissue-damage using the *ex vivo* model of BP. Interestingly, using SOD as a scavenger for superoxide we could not limit the destructive capacity of granulocytes. Possible explanations for this effect may include but are not limited to the following: 1) the superoxide is not the most important player in this process. Given its short half-life it would rather be expected that other longer-lived ROS may be the power horses in the process upon which “respiratory burst” is initiated; 2) The residual superoxide might enter the reactions with H_2O_2 at different rates and generate more powerful radicals/oxidants like the singlet, the hydroxyl and hydroxy that could represent a reservoir for further reaction with the eventual production of more stable oxidants like the hypochlorous acid. 3) Despite its intended use as a scavenging agent, the SOD might be responsible for generating huge amounts of H_2O_2 that cannot be timely-efficiently neutralized by the limited amount of catalase present in stimulated granulocytes. Thus in the scenario where superoxide is not the principal effector, an inverse effect is seen i.e., the scavenging of superoxide results in an increased pathogenic potential. Actually, a comparable effect has been previously seen in *ex vivo* experiments using another combination of sera, skin and SOD (Chiriac *et al.*, unpublished observations). However, in that study, none of these possible scenarios was specifically addressed. In order to provide novel experimental data we investigated the scavenging potential of SOD in phorbol 12-myristate 13-acetate (PMA)-stimulated granulocytes using a luminometric assay as described below.

SOD scavenges most of but not all of the superoxide anion produced by PMA-stimulated granulocytes

To further delineate the possible mechanism underlying the inability of SOD to limit blistering, we performed a dose-dependent inhibition assay in PMA-stimulated granulocytes using luminol. The principle of the method is based on the ability of the superoxide anion to oxidize luminol in a reaction producing photons that can be readily measured with a standard luminometer (Wang *et al.*, 1991). We found that 1500 U/ml SOD were sufficient to remove more than 85 % of the superoxide produced by PMA-activated granulocytes (Figure 3). In an attempt to reach an even higher percentage of inhibition, we tested different SOD concentrations ranging from 100 to 2000 U/ml. However, no higher rates were observed with any of the other concentrations (not shown).

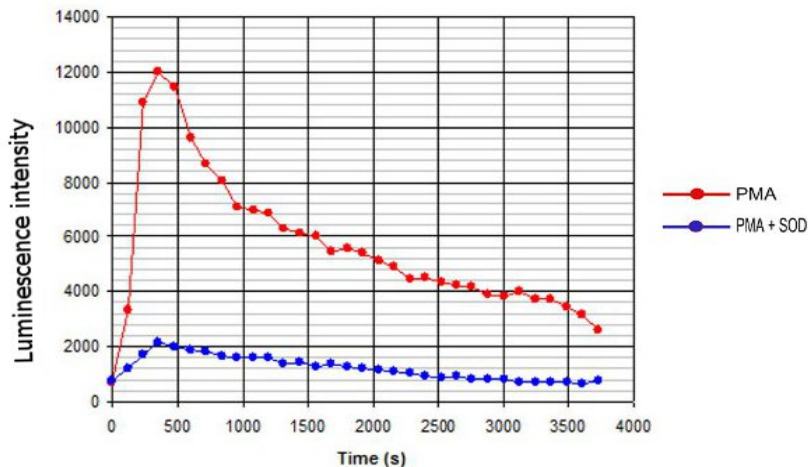


Figure 3. SOD removes most of the superoxide anion produced by PMA-activated granulocytes. Incubation of human granulocytes with 500 nM PMA induced a respiratory burst as revealed by the superoxide-dependent oxidation of luminol. Co-incubation of granulocytes with 1500 U/ml SOD prior to their stimulation with 500 nM PMA led to an 85% drop in the superoxide production.

ROS produced by activated neutrophils are crucial for the defense against pathogenic microorganisms. ROS protection against infection is underlined by the fact that patients with chronic granulomatous disease characterized by an inherited defect in phagocyte superoxide production have an increased susceptibility to infections (Pollock *et al.*, 1995; Jackson *et al.*, 1995). Along with their benefic effects in antimicrobial defense, the destructive effects of ROS on self tissues have long been recognized (Chiriac *et al.*, 2007). In autoimmune diseases the role of ROS in tissue damage is still controversial. Superoxide anion is very rapidly converted to hydrogen peroxide by the SOD, an antioxidant enzyme which protects leukocytes and other cells from being damaged by the superoxide resulted in the physiologic process of

cellular respiration or due to other environmental factors such as ultraviolet radiation. Enhancement of the superoxide removal by administration of SOD mimetics reduced chronic inflammation and tissue and bone damage associated with collagen induced arthritis in the rat (Cuzzocrea *et al.*, 2005). Here we show that in the *ex vivo* model of bullous pemphigoid addition of bovine SOD could not protect from granulocyte-dependent DES. This finding suggests that the superoxide anion, despite its short-live nature may generate other reactive oxygen species which can induce tissue damage. On the other hand it has been reported that antibodies generate ozone that has been found functional in bacterial killing and inflammation by another mechanism thus short-cutting the classical pathway discussed above (Wentworth *et al.*, 2003). A similar event may also be responsible for the clinical outcome in autoimmune diseases. Furthermore, cells possess 3 kinds of SOD, the involvement of which might be regulated in a fine spatial-temporal manner by as yet unrevealed control mechanisms. The imitation of such a complex situation *ex vivo* might need further efforts that could be addressed in further studies.

Myeloperoxidase inhibition resulted in a reduction of split formation by pathogenic antibodies-activated granulocytes

Myeloperoxidase is the most abundant protein in neutrophils which catalyzes the conversion of H_2O_2 and chloride into HOCl, the most powerful oxidant produced by these cells. To investigate the role of MPO in the *ex vivo* DES model induced by antibody-activated granulocytes we inhibited the enzyme activity using 4-aminobenzoic acid hydrazide (ABAH) a very specific and effective MPO inhibitor (Kettle *et al.*, 1997). Addition of 100 μM ABAH to the granulocyte suspension which was subsequently added to the skin cryosections, substantially decreased the tissue destruction capacity (Figure 4a) compared to our positive control where no inhibitor was added (Figure 4b). As expected, DES was not induced by the serum antibodies from healthy donors (Figure 4c). This interesting observation is in line with previous observations suggesting that a dose-dependent inhibition of the MPO activity might parallel the blister-blocking potential of antibody-activated granulocytes (Chiriac *et al.*, unpublished observations).

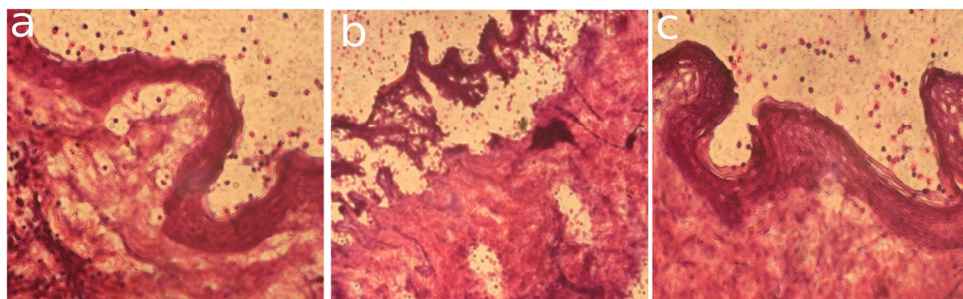


Figure 4. MPO inhibition by ABAH resulted in a decreased DES. (a) Addition of 100 μM ABAH to the granulocytes before their incubation with skin cryosections treated with pathogenic antibodies induced a less intense DES in comparison with (b) the cryosections where no inhibitor was added. (c) No separation was induced by serum from healthy donors.

Conclusions

Taken together our present data provide further evidence for the implication of ROS in the autoantibody-induced granulocyte-dependent tissue-damage in experimental BP. These results demonstrate that SOD and AHAB differently modulate the tissue-damaging capacity of BP autoantibodies in the *ex vivo* model of BP. Nevertheless, a better characterization of the fine molecular pathways triggered by the antibody-dependent neutrophil activation in the context of chronic inflammation will facilitate our understanding of disease pathogenesis identifying novel molecular targets for specific therapies.

Acknowledgements

This work was supported by grants IDEI_1146/2009, PCCE_ID_312/2008 and PCCE_ID_129/2008 by the Romanian National Council for Scientific Research in Higher Education and grants from the Deutsche Forschungsgemeinschaft SI-1281/2-1 and SI-1281/4-1(to CS). EL received financial support from the Sectorial Operational Programme for Human Resources Development 2007-2013, co-financed by the European Social Fund, under the project number POSDRU 6/1.5/S/3 (Doctoral studies: through science towards society).

REFERENCES

- Arvadia, P., Narwaley, M., Whittal, R.M., Siraki, A.G. (2011) 4-aminobenzoic acid hydrazide inhibition of myeloperoxidase-11: catalytic inhibition by reactive metabolites. *Arch. Biochem. Biophys.*, **515**, 120-126.
- Caldefie-Chézet, F., Walrand, S., Moinard, C., Tridon, A., Chassagne, J., Vasson, M. (2002) Is the neutrophil reactive oxygen species production measured by luminol and lucigenin chemiluminescence intra or extracellular? comparison with dcfh-da flow cytometry and cytochrome c reduction. *Clin. Chim. Act.*, **319**, 9-17.
- Chen, R., Fairley, J.A., Zhao, M., Giudice, G.J., Zillikens, D., Diaz, L.A., Liu, Z. (2002) Macrophages, but not t and b lymphocytes, are critical for subepidermal blister formation in experimental bullous pemphigoid: macrophage-mediated neutrophil infiltration depends on mast cell activation, *J. Immunol.*, **169**, 3987-3992.
- Chen, R., Ning, G., Zhao, M.L., Fleming, M. G., Diaz, L.A., Werb, Z., Liu, Z. (2001) Mast cells play a key role in neutrophil recruitment in experimental bullous pemphigoid, *J. Clin. Invest.*, **108**, 1151-1158.
- Chiriac, M.T., Roesler, J., Sindrilariu, A., Scharffetter-Kochanek, K., Zillikens, D., Sitaru, C. (2007) NADPH oxidase is required for neutrophil-dependent autoantibody-induced tissue damage, *J. Pathol.*, **212**, 56-65.

- Csorba, K., Sesărman, A., Oswald, E., Feldrihan, V., Fritsch, A., Hashimoto, T., Sitaru, C. (2010) Cross-reactivity of autoantibodies from patients with epidermolysis bullosa acquisita with murine collagen vii, *Cell. Mol. Life Sci.*, **67**, 1343-1351.
- Cuzzocrea, S., Mazzon, E., Paola, R.D., Genovese, T., Muià, C., Caputi, A.P., Salvemini, D. (2005) Effects of combination m40403 and dexamethasone therapy on joint disease in a rat model of collagen-induced arthritis, *Arthritis Rheu.*, **52**, 1929-1940.
- Dvorak, A.M., Mihm, M.C.J., Osage, J.E., Kwan, T.H., Austen, K.F., Wintroub, B.U. (1982) Bullous pemphigoid, an ultrastructural study of the inflammatory response: eosinophil, basophil and mast cell granule changes in multiple biopsies from one patient, *J. Invest. Dermatol.*, **78**, 91-101.
- Gammon, W.R., Merritt, C.C., Lewis, D.M., Sams, W.M., Wheeler, C.E., Carlo, J. (1981) Leukocyte chemotaxis to the dermal-epidermal junction of human skin mediated by pemphigoid antibody and complement: mechanism of cell attachment in the in vitro leukocyte attachment method., *J. Invest. Dermatol.*, **76**, 514-522.
- Gammon, W.R., Merritt, C.C., Lewis, D.M., Sams, W.M.J., Carlo, J.R., Wheeler, C.E.J. (1982) An in vitro model of immune complex-mediated basement membrane zone separation caused by pemphigoid antibodies, leukocytes, and complement, *J. Invest. Dermatol.*, **78**, 285-290.
- Hultqvist, M., Olofsson, P., Holmberg, J., Backstrom, B.T., Tordsson, J., Holmdahl, R. (2004) Enhanced autoimmunity, arthritis, and encephalomyelitis in mice with a reduced oxidative burst due to a mutation in the *cf1* gene., *Proc. Natl. Acad. Sci. USA.*, **101**, 12646-12651.
- Jackson, S.H., Gallin, J.I., Holland, S.M. (1995) The p47phox mouse knock-out model of chronic granulomatous disease, *J. Exp. Med.*, **182**, 751-758.
- Kettle, A.J., Gedye, C.A., Winterbourn, C.C. (1997) Mechanism of inactivation of myeloperoxidase by 4-aminobenzoic acid hydrazide, *Biochem. J.*, **321** (Pt 2), 503- 508.
- Lessey, E., Li, N., Diaz, L., Liu, Z. (2008) Complement and cutaneous autoimmune blistering diseases, *Immunol. Res.*, **41**, 223-232.
- Liu, Z., Diaz, L.A., Troy, J.L., Taylor, A.F., Emery, D.J., Fairley, J.A., Giudice, G.J. (1993) A passive transfer model of the organ-specific autoimmune disease, bullous pemphigoid, using antibodies generated against the hemidesmosomal antigen, bp180, *J. Clin. Invest.*, **92**, 2480-2488.
- Liu, Z., Giudice, G.J., Swartz, S.J., Fairley, J.A., Till, G.O., Troy, J.L., Diaz, L.A. (1995) The role of complement in experimental bullous pemphigoid, *J. Clin. Invest.*, **95**, 1539-1544.
- Liu, Z., Shapiro, S.D., Zhou, X., Twining, S.S., Senior, R.M., Giudice, G.J., Fairley, J.A., Diaz, L.A. (2000) A critical role for neutrophil elastase in experimental bullous pemphigoid, *J. Clin. Invest.*, **105**, 113-123.
- Mihai, S., Sitaru, C. (2007) Immunopathology and molecular diagnosis of autoimmune bullous diseases, *J. Cell. Mol. Med.*, **11**, 462-481.

- Nelson, K.C., Zhao, M., Schroeder, P.R., Li, N., Wetsel, R.A., Diaz, L.A., Liu, Z. (2006) Role of different pathways of the complement cascade in experimental bullous pemphigoid, *J. Clin. Invest.*, **116**, 2892-2900.
- Nishie, W., Sawamura, D., Goto, M., Ito, K., Shibaki, A., McMillan, J.R., Sakai, K., Nakamura, H., Olasz, E., Yancey, K.B., Akiyama, M., Shimizu, H. (2007) Humanization of autoantigen, *Nat. Med.*, **13**, 378-383.
- Nishie, W., Sawamura, D., Natsuga, K., Shinkuma, S., Goto, M., Shibaki, A., Ujiie, H., Olasz, E., Yancey, K.B., Shimizu, H. (2009) A novel humanized neonatal autoimmune blistering skin disease model induced by maternally transferred antibodies, *J. Immunol.*, **183**, 4088-4093.
- Olasz, E.B., Yancey, K.B. (2008) Bullous pemphigoid and related subepidermal autoimmune blistering diseases, *Curr. Dir. Autoimmun.*, **10**, 141-166.
- Pollock, J.D., Williams, D.A., Gifford, M.A., Li, L.L., Du, X., Fisherman, J., Orkin, S.H., Doerschuk, C.M., Dinauer, M.C. (1995) Mouse model of x-linked chronic granulomatous disease, an inherited defect in phagocyte superoxide production, *Nat. Genet.*, **9**, 202-209.
- Ross, A.D., Banda, N.K., Muggli, M., Arend, W.P. (2004) Enhancement of collagen-induced arthritis in mice genetically deficient in extracellular superoxide dismutase, *Arthritis Rheum.*, **50**, 3702-3711.
- Sitaru, C. (2009) Bullous pemphigoid: a prototypical antibody-mediated organ-specific autoimmune disease, *J. Invest. Dermatol.*, **129**, 822-824.
- Sitaru, C., Kromminga, A., Hashimoto, T., Bröcker, E. B., Zillikens, D. (2002a) Autoantibodies to type vii collagen mediate fcgamma-dependent neutrophil activation and induce dermal-epidermal separation in cryosections of human skin, *Am. J. Pathol.*, **161**, 301-311.
- Sitaru, C., Schmidt, E., Petermann, S., Munteanu, L.S., Bröcker, E., Zillikens, D. (2002b) Autoantibodies to bullous pemphigoid antigen 180 induce dermal-epidermal separation in cryosections of human skin, *J. Invest. Dermatol.*, **118**, 664-671.
- van der Veen, R.C., Dietlin, T.A., Hofman, F.M., Pen, L., Segal, B.H., Holland, S.M. (2000) Superoxide prevents nitric oxide-mediated suppression of helper t lymphocytes: decreased autoimmune encephalomyelitis in nicotinamide adenine dinucleotide phosphate oxidase knockout mice, *J. Immunol.*, **164**, 5177-5183.
- Wang, J.F., Komarov, P., Sies, H., de Groot, H. (1991) Contribution of nitric oxide synthase to luminol-dependent chemiluminescence generated by phorbol-ester-activated kupffer cells, *Biochem. J.*, **279** (Pt 1), 311-314.
- Wentworth, P.J., Nieva, J., Takeuchi, C., Galve, R., Wentworth, A.D., Dille, R.B., DeLaria, G.A., Saven, A., Babior, B.M., Janda, K.D., Eschenmoser, A., Lerner, R.A. (2003) Evidence for ozone formation in human atherosclerotic arteries, *Science*, **302**, 1053- 1056.
- Yancey, K.B. (2005) The pathophysiology of autoimmune blistering diseases, *J. Clin. Invest.*, **115**, 825-828.

EFFECTS OF ZINC, LEAD AND CADMIUM POLLUTION ON THE STRUCTURE AND ACTIVITIES OF SOIL BACTERIAL COMMUNITY

CODRUȚA VIOLETA SIMULE^{1,✉} and MIHAIL DRĂGAN BULARDA²

SUMMARY. The impact of human activities on soil quality has increased over the past decades due to population growth and extensive exploitation of natural resources, including soils. Chemical tests measure the amount of pollutants but they do not reflect the environmental consequences resulting from their mobilization, accumulation along the food chain and specially their impact on key metabolic processes in the soil. Biological methods, in turn, reflect the impact on the organisms from the soil, thus showing enhancement / inhibition of the activities under stress conditions. In order to establish the effect of pollutants on edaphic soil communities of microorganisms, the ecophysiological group dynamics of bacteria and enzymatic activities were analyzed in the presence of different concentrations of environmental pollutants (zinc, lead and cadmium). This study allowed and identification of bacterial parameters sensitive to pollution. Bacterial density and intensity of enzymatic activities showed quantitative variations depending on the type and concentration of metal. The most sensitive to pollution were found to be nitrifying bacteria and dehydrogenase activities.

Keywords: bacterial communities, enzymatic activities, heavy metals, soil pollution.

Introduction

Soil is a dynamic system that is vital to human activities and to maintaining ecosystems. As an interface between the earth's crust, atmosphere and hydrosphere, the soil is a non-renewable resource that fulfils many vital functions: biomass production, storage, filtering and transformation of organic substances and minerals; source of biodiversity, habitats and species; physical environment for people and human activities; source of raw materials.

In the evolutionary sense, microorganisms (primarily heterotrophic microorganisms) are recycling agents responsible for maintaining the biosphere. These agents develop favorable, thermodynamic chemical reactions obtaining energy and carbon from

^{1,✉} **Corresponding author**, Ministry of Environment and Forests, Intermediate Body Cluj-Napoca, 47 Minerilor Street, 400406/Cluj-Napoca, Romania, E-mail: codruta.simule@yahoo.com

² Babes-Bolyai University, 1 Kogălniceanu Street, 400084/Cluj-Napoca, Romania, E-mail: draganb@bioge.ubbcluj.ro

dead biomass. As a result of microbial processes of decomposition, the essential nutrients present in the biomass of one generation of organisms are available for the next generation.

Microbial survival in polluted soils depends on intrinsic biochemical and structural properties, physiological, and/or genetic adaptation including morphological changes of cells, as well as environmental modifications of metal speciation (Wuertz and Mergeay, 1997). For example, high levels of heavy metals can affect the qualitative as well as quantitative composition of microbial communities. Several studies have found that metals influence microorganisms by harmfully affecting their growth, morphology, and biochemical activities, resulting in decreased biomass and diversity (Malik and Ahmed, 2002). Previous studies have shown that long term (Duxbury and Bicknell, 1983) and short term (Wickham *et al.*, 1988) stresses such as high temperature, extremes of pH or chemical pollution often result in altered metabolism, species diversity and plasmid incidence of soil bacteria populations (Bahig *et al.*, 2008).

The aims of this study is to argument from a scientific point of view the need to include biological parameters in studies of environmental impact assessment and in the national strategies for soil quality monitoring, practices that currently are based only on the determination of physical and chemical parameters.

Given the fact that the soil is subjected to strong anthropogenic influence, it is of major importance to establish the effect of pollutants on edaphic soil communities of microorganisms.

Materials and methods

Soil samples. The samples were taken from the Cheile Turzii Nature Reserve, one of the most important protected wildlife sites in Cluj County. Individual soil cores were taken with a PVC core sampler (at a depth of 0-20 cm) from three different places and mixed together to prepare a composite sample for each site. The composite samples were kept under natural conditions for 30 days, after which was evaluated the effect of heavy metals applied (Zn, Pb, Cd) on the aerobic heterotrophic bacteria, ammonifying bacteria, nitrifying bacteria, denitrifying bacteria, iron-reducing bacteria and sulphate reducing bacteria; on dehydrogenase, phosphatase, catalase and urease activities; and on soil respiration.

Microbiological analyses. The following 7 ecophysiological groups of bacteria were analyzed: aerobic heterotrophic bacteria, ammonifying bacteria, nitrifying bacteria, denitrifying bacteria, iron-reducing bacteria, and sulphate reducing bacteria.

A solid nutrient medium containing meat extract, 0.3 g; agar-agar, 2 g; peptone, 1 g; NaCl, 0.5 g and 100 ml distilled water, was used for enumeration of the total number of *aerobic heterotrophic bacteria* (Atlas, 2004). The pH was adjusted to 7.5, prior sterilization at 120°C for 1 hour.

Ammonifying bacteria were revealed in liquid culture medium containing peptone, 2 g; NaCl, 0.5 g; 100 ml distilled water (Drăgan-Bularda medium) (Drăgan-Bularda, 2000). The pH was adjusted to 7.9 before sterilization at 120°C for 1 hour.

Ammonium oxidizing bacteria were cultured on a liquid culture medium containing Winogradsky's salt solution (0.4 g K_2HPO_4 , 0.13 g NaCl, 0.13 g $MgSO_4 \cdot 7H_2O$, 1.52 mg $MnSO_4 \cdot H_2O$, 0.5 g NH_4NO_3) diluted 1:20, 100 ml; ammonium sulphate $(NH_4)_2SO_4$, 0.05 g, calcium carbonate ($CaCO_3$), 0.1 g (Drăgan-Bularda medium) (Drăgan-Bularda, 2000). The medium was sterilized at 110 °C for 20 minutes.

For *nitrite-oxidizing bacteria*, the following liquid culture medium was used: Winogradsky's salt solution diluted 1:20, 100 ml; sodium nitrate ($NaNO_3$), 0.1 g; calcium carbonate ($CaCO_3$), 1 g (Drăgan-Bularda medium, 2000). The medium was sterilized at 110 °C for 20 minutes.

A liquid culture medium consisted of: potassium nitrate (KNO_3), 0.2 g; glucose, 1 g; $CaCO_3$, 0.5 g; *Winogradsky's salt solution*, 5 ml and distilled water, 95 ml; pH, 7.2 (De Barjac culture medium) (Pochon, 1954) was used to enumerate *denitrifying bacteria*. The medium was sterilized at 112 °C for 20 minutes on three successive days.

Iron-reducing bacteria were cultured in a liquid culture medium that contained glucose, 2 g; asparagines, 0.5 g; yeast extract, 0.05 g; dibasic potassium phosphate (K_2HPO_4), 0.3 g; monobasic potassium phosphate (KH_2PO_4), 0.08 g; potassium chloride (KCl), 0.02 g; distilled water 100 ml, iron oxide ($Fe_2O_3 \cdot 3H_2O$), 0.1g; pH, 7.0 (Ottow medium, 1968). The medium was sterilized at 105 °C for 1 hour on three successive days.

Sulfate reducing bacteria were revealed in a liquid culture medium with Na-lactate, 0.5 g; asparagines, 0.2 g; dibasic potassium phosphate (K_2HPO_4), 0.1 g; trace metal solution (0.15 g $MgSO_4 \cdot 7H_2O$, $FeSO_4 \cdot 7H_2O$); distilled water, 100 ml (Van Delden medium) (Allen, 1957). The medium was sterilized at 105 °C for 1 hour on three successive days.

Total viable counts of culturable aerobic heterotrophic bacteria were obtained by preparing six successive 10-fold serial dilutions of 1 g of fresh soil samples (in order to obtain a small number of colonies on each plate) and surface plating on to sterile nutrient agar in triplicate. After incubation (30°C for 7 days), the counts obtained were multiplied by the dilution factor to obtain the number of colony forming unit per gram of soil.

Except for the aerobic heterotrophic bacteria (where the plate count method was used), the most probable number (MPN) method was applied to estimate the number of soil microorganisms, using dilution series and multiple tubes per dilution (five tubes for each of the six successive 10-fold dilutions). Dilution was made until a readable count was obtained. After incubation, the most probable number of bacteria was calculated according to the statistical table of Alexander (1965).

Enzymological analyses. The activities of following five enzymes were studied according to Drăgan-Bularda (2000): phosphatase – activity expressed in mg phenol/g dry matter soil; catalase – activity expressed in mg splitted H_2O_2 /g dry matter soil; urease – activity expressed in mg NH_4 /g dry matter soil; actual and potential dehydrogenase – activities expressed in mg formazan/g dry matter soil.

The analytical data serves as the base for calculating the bacterial (BISQ) (Muntean, 1995-1996) and enzymatic indicator of the soil quality (EISQ) (Muntean *et al.*, 1996; 2006).

Soil respiration. Overall physiological activity of microorganisms in the analyzed soil samples, expressed through soil respiration level, was determined by assessing the amount of CO_2 emitted by the total spectrum of microorganisms in the sample, using a system consisting of a room from soil respiration type SRC-1, coupled with an CO_2 analyzer tip EGM -4.

Heavy metals. The following salts of heavy metals were used in this study: $ZnSO_4 \times 7H_2O$, $(CH_3COO)_2Pb \times 3H_2O$ and $Cd(NO_3)_2 \times 4H_2O$. Heavy metal concentrations were chosen according to the maximum permitted by applicable law in force (Order no. 756/1997). The numbering system from I to VI for the metal concentrations tested, as detailed in Table 1 is used throughout the paper to simplify the presentation of results.

Table 1.

Heavy metal concentrations (Zn, Pb and Cd) used in evaluation of the impact on microbial soil population

Used concentration	Zinc (mg/kg)	Lead (mg/kg)	Cadmium (mg/kg)
I	10	5	0.5
II	20	10	1
III	100	20	5
IV	150	40	10
V	200	70	15
VI	400	140	20

Statistical analysis. The results obtained were examined statistically with a one-way analysis of variance (ANOVA). The least significant differences were calculated with the Tukey's test at a significance level of $p=0.05$ and $p=0.01$. Pearson's correlation coefficient r was used to describe the degree of linear association between the cell viability and soil metal concentrations.

Results and discussion

Impact of pollution with zinc, lead and cadmium on the size of microbial population from the soil. In the case of eco-physiological groups of bacteria studied, there were highlighted numerical fluctuations depending on the type and concentration of metal in which was added (Fig. 1-3).

The obtained results showed that the addition of pollutants in soil, on different groups of eco-physiological microorganisms had different types of response. Adding Zn, Pb and Cd in low concentration had a slightly stimulatory or inhibitory effect, while application of high concentrations of heavy metals had a strong inhibitory effect.

Aerobic heterotrophic bacteria were most resistant to pollution, maintaining themselves even in the presence of elevated concentrations of metals (Zn IV, Pb VI, Cd VI) and nitrifying bacteria were most susceptible, followed by denitrifying bacteria and iron-reducing bacteria. In the presence of heavy metals at the same concentrations (10 and 20 mg/kg), the number of ammonium oxidizing bacteria was reduced by 45.77 to 100% and the number of nitrite-oxidizing bacteria by 42.34 to 100%, compared to the control sample (100%).

Due to the sensitivity shown by nitrifying bacteria to heavy metal pollution, we recommend including this group of bacteria in assessment and monitoring of polluted soils studies.

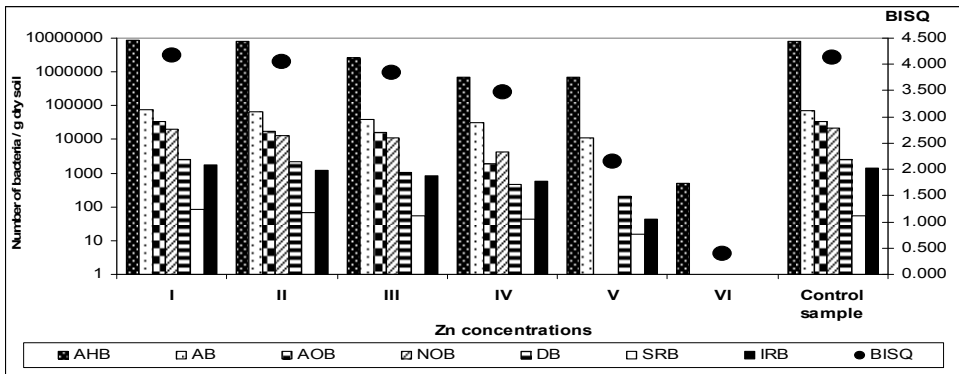


Fig. 1. Zn effect on bacteria number from samples collected from Cheile Turzii during summer of 2010 after 30 days of incubation. Metal concentrations: see Tab.1.

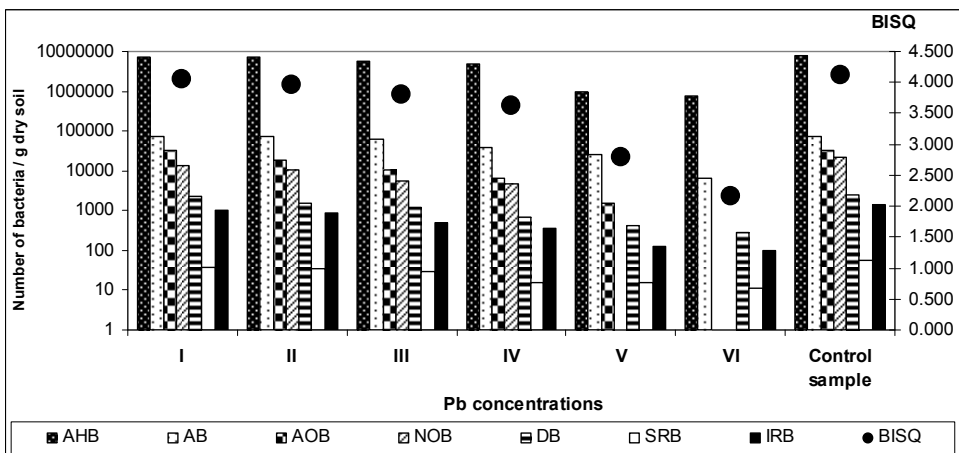


Fig. 2. Pb effect on bacteria number from samples collected from Cheile Turzii during summer of 2010 after 30 days of incubation. Metal concentrations: see Tab.1.

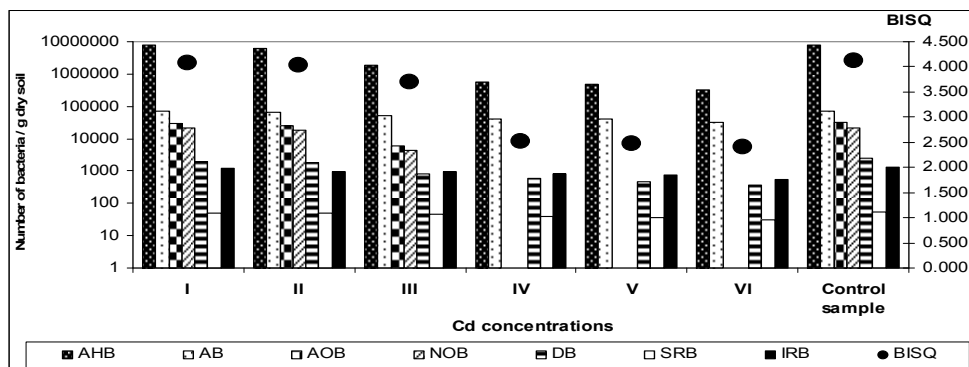


Fig. 3. Cd effect on bacteria number from samples collected from Cheile Turzii during summer of 2010 after 30 days of incubation. Metal concentrations: see Tab.1.

Aerobic heterotrophic bacteria (AHA), ammonifying bacteria (AB), ammonium oxidizing bacteria (AOB), nitrite-oxidizing bacteria (NOB) and denitrifying bacteria (DB) were more sensitive to Cd than for Pb, while sulphate reducing bacteria (SRB) and iron-reducing bacteria (IRB) showed a higher sensitivity for Pb.

The harmful effect of metals was obvious, in all eco-physiological studied groups studied values recorded in samples with high concentrations of Zn, Pb and Cd were lower than in samples with low concentrations and maximum values were recorded in the control sample, without added metals. This effect is even more meaningfully pictured by the values of the bacterial indicator of soil quality (BISQ), calculated based on the number of bacteria belonging to all analyzed eco-physiological groups (Muntean, 1995-1996) (Fig. 4).

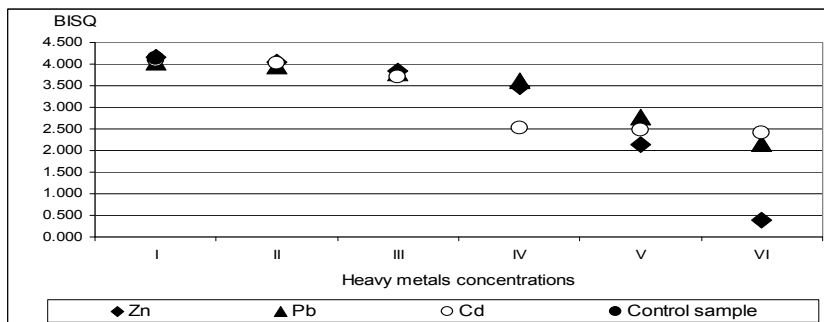


Fig. 4. BISQ evolution under the action of heavy metals (Zn, Pb, Cd) Metal concentrations: see Table. 1.

The values for BISQ are comprised between 4.127 and 0.386, with a gradual downward trend, according to the growing concentration of metal in the soil. The maximum value (4.127) was calculated for the control sample without the addition of metals and the minimum values in samples Cd VI (2.401), Pb VI (2.167) and Cd VI (0.385), respectively.

The impact of pollution with zinc, lead and cadmium on enzymatic activities. In this study was investigated the effect of zinc, lead and cadmium on two oxidoreductases: catalase (CA) and dehydrogenase (actual dehydrogenase - ADA and potential dehydrogenase - PDA) and two hydrolases, involved in the cycling of N (urease – UA) and P (phosphatase - PA).

All analyzed enzymatic activities were identified in all samples, with variations depending on the type of metal and its concentration.

The analyzed enzymatic activities were sensitive to pollution with Zn, Pb and Cd, aspect reflected by the analysis of EISQ evolution. However, dehydrogenase was more sensitive to pollution with heavy metals, which recommends its inclusion in soil quality assessments, along with nitrifying bacteria. The intensity of dehydrogenase activity was reduced, in the presence of heavy metals at the same concentrations, up to 97.18% compared to the control sample (100%) (Fig. 5-7).

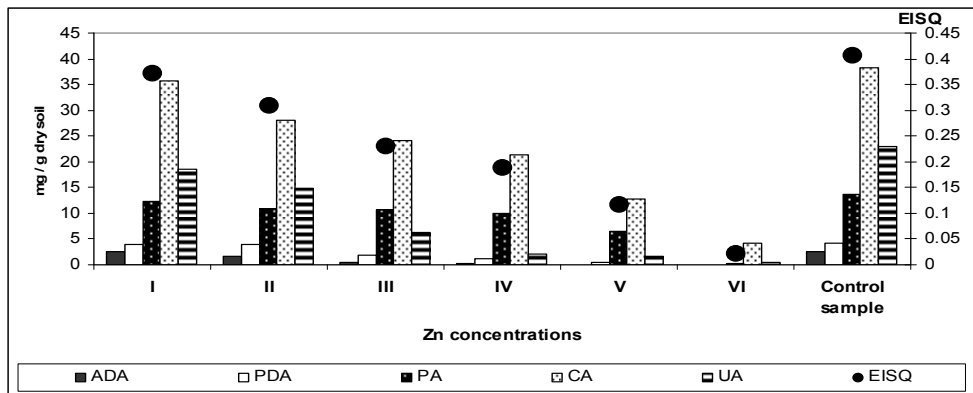


Fig. 5. Zn effect on the intensity of enzymatic activities in samples collected from Cheile Turzii during summer of 2010 after 30 days of incubation. Metal concentration: see Tab. 1.

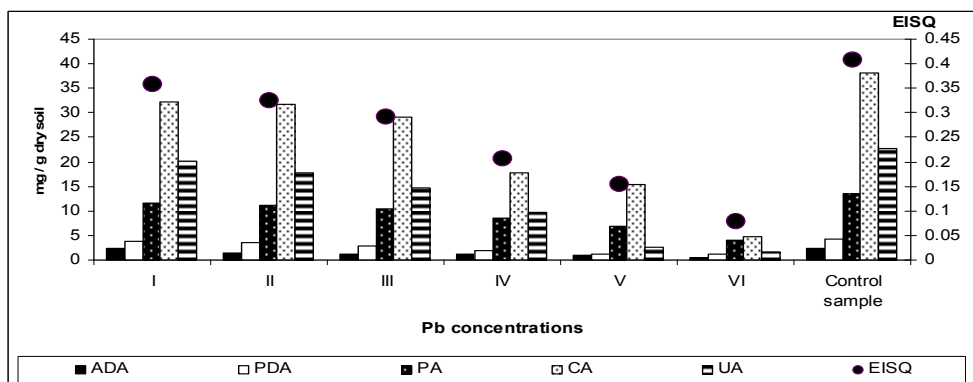


Fig. 6. Pb effect on the intensity of enzymatic activities in samples collected from Cheile Turzii during summer of 2010 after 30 days of incubation. Metal concentration: see Tab. 1.

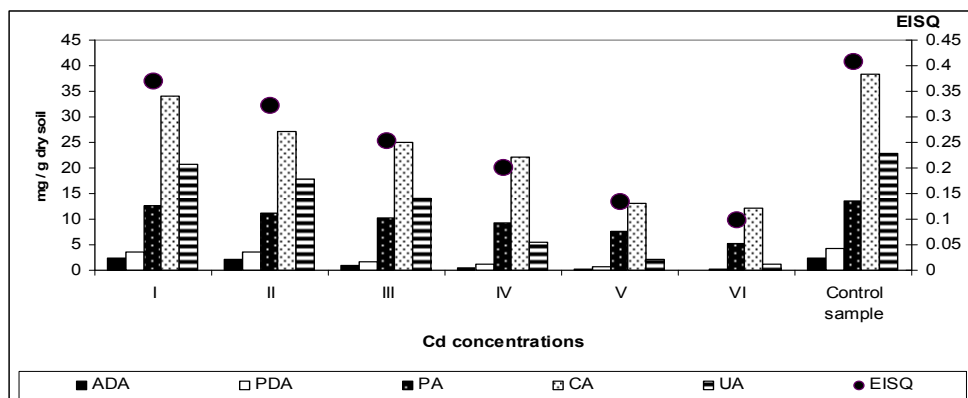


Fig. 7. Cd effect on the intensity of enzymatic activities in samples collected from Cheile Turzii during summer of 2010 after 30 days of incubation. Metal concentration: see Tab. 1.

The increased sensitivity of dehydrogenase activity to metal contamination can be explained by the fact that the dehydrogenase is active only within living cells, intact, unlike other enzymes that act outside the cell. Dehydrogenase activity was most sensitive to pollution with Cd, followed by Pb and Zn.

The phosphatase and catalase were the most tolerant, phosphatase being more sensitive than catalase in the presence of Zn and Pb and tolerant in the presence of Cd.

There was a gradual reduction of EISQ recorded, during the growing concentration of heavy metals added to the soil samples, due to the inhibitory effect of pollutants on all enzyme activities (Fig. 8).

The enzymatic indicator of the analyzed samples offers an overall image on the intensity of the enzymatic activity and, implicitly, of the general biological activity in the analyzed soils. The enzymatic indicator may have values ranging between 0 (when no real activity of any of the studied enzymes is detected) and 1 (when all the activities have real individual values equal to the maximum theoretic values).

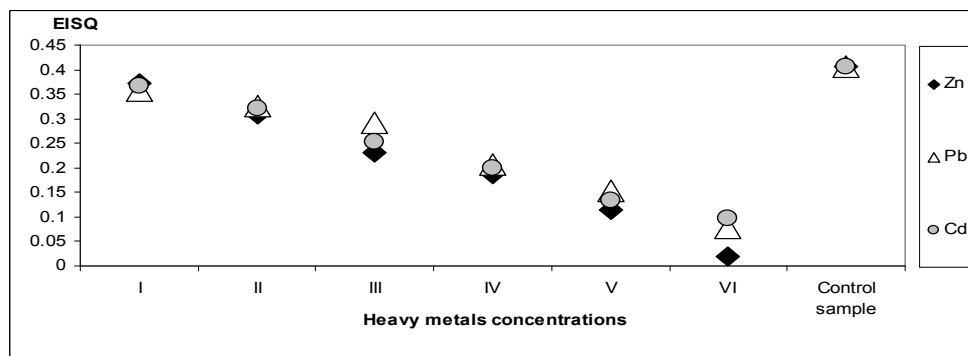


Fig. 8. EISQ evolution under the action of metals added in different concentrations. Metal concentration: see Tab. 1.

The enzymatic indicator of soil quality (EISQ) does not reach in any of the samples the maximum theoretic value (1), but varies between 0.407 and 0.02. The maximum value (0.407) was recorded in the control sample and the minimum in the Cd VI (0.097), Pb VI (0.079) and Zn VI (0.02) samples.

The impact of pollutions with zinc, lead and cadmium on soil respirations. Soil respiration was higher in less polluted soils than in the polluted ones. However, the amount of CO₂ significantly decreasing only at high concentrations of heavy metals (Fig. 9).

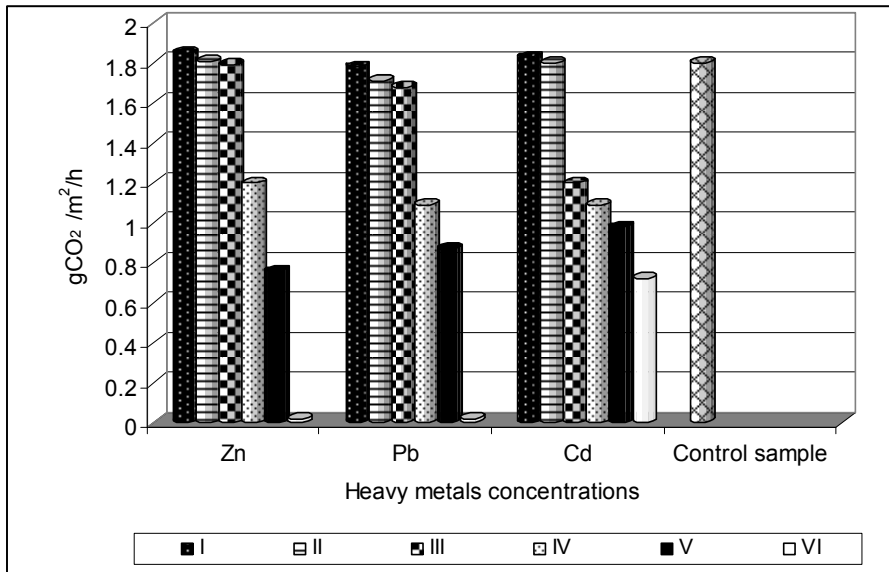


Fig. 9. The effect of different heavy metal concentrations (Zn, Pb, Cd) on soil respiration after 30 days of incubation.
Metal concentration: see Tab. 1.

Therefore, soil respiration may be a useful indicator in studies of assessment and monitoring of heavy metals impact on microorganisms, but preferably in conjunction with other indicators, because it can be stimulated in case of pollution, while other parameters are inhibited.

Statistical analysis of data showed the existence of negative correlations, statistically significant, between all eco-physiological groups of bacteria, enzymatic activities, soil respiration and concentration of heavy metals (Zn, Pb and Cd). Positive correlations, statistically significant, were detected between the size of bacterial populations and enzyme activities, respectively soil respiration.

Conclusions

Study of changes in the structure and activities of soil bacterial community is an important component of soil toxicity and bioassessment tests. This study makes a real contribution on the effect of anthropogenic influences on soil quality, their relationship with microbial activity and enzymatic potential, all these leading to the identification of bacterial parameters sensitive to pollution.

In the present investigation, bacterial density and intensity of enzymatic activities showed quantitative variations depending on the type and concentration of metal. These data are comparable with other observations effected on microbial populations under lab conditions (Ahmad *et al.*, 2005). The most sensitive to pollution were found to be nitrifying bacteria and dehydrogenase activities.

The presence of elevated concentrations of metals had a strong inhibitory effect on resistant species and caused the death of those susceptible to pollution. These toxic effects show that resistance mechanisms do not provide protection from high levels of metals.

In conclusion, because of their many capacities, the use of microorganisms in the assessment and monitoring programs are necessary, changes in the micro-flora of a specific site indicating changes in environmental quality. To capture as closely as possible changes caused by human impact several indicators must be used (measurements of microbial biomass, respiration, key microorganisms, enzyme activities, etc.).

Soil enzymes are considered to be sensitive indicators of contamination because of their role in organic matter cycling and regulation of nutrient pools (Visser and Parkinson, 1992). Enzyme activities in the soil change earlier than other parameters. Therefore, the determination of enzyme activities are more appropriate, thus providing suggestive data in a much shorter time than microbiological analysis on biodegradable processes in soil.

Having regard the crucial role of soil, which is actually an essential active mediator of performing processes that is at the basis of life on earth, is necessary and extremely important to biomonitoring in a complex way soil quality in order to identify and remove the sources of pollution and thus maintain a maximum ecological potential. A precise bio-monitoring is essential in anticipating risks for the environment and human health.

However, deep future studies are needed for understanding of the genetic diversity of microbial populations sensitive and tolerant to metal and metal-microorganism interactions in soil in natural conditions.

REFERENCES

- Ahmad, I., Hazat, S., Ahmad, A., Inam, A., Smiullah, A. (2005) Effect of heavy metal on survival of certain groups of indigenous soil microbial population, *J. Appl. Sci. Environ*, **9** (1), 115-121.

- Alexander, M. (1965) *Most probable number method for microbial populations*, în Black, C.A., Evans, D.D., White, J.L., Ensminger, L.E., Clark, F. E. (Eds.), *Methods of Soil Analysis*, pp. 1467-1472, Am. Soc. Agron., Madison, Wisconsin.
- Allen, O.N. (1957) *Experiments in Soil Bacteriology, 3rd edition*, Ed. Burgess, Minneapolis, Minnesota.
- Atlas, R.M. (2004) *Handbook of Microbiological Media, 3rd edition*, CRC Press, New York.
- Bahig, A.E., Aly, E.A., Khaled, A.A., Amel, K.A. (2008) Isolation, characterization and application of bacterial population from agricultural soil at Sohag Province, *Egypt Malaysian J. Microbiol.*, **4** (2), 42-50.
- Drăgan-Bularda, M. (2000) *Microbiologie generală – lucrări practice*, Ed.III, Cluj-Napoca.
- Duxbury, T. and Bicknell, B. (1983) Metal tolerant bacterial populations from natural and metal-polluted soils. *Soil Biol. Biochem.*, **15**, 243–250.
- Malik, A., Ahmed, M. (2002) Seasonal variation in bacterial flora of the wastewater and soil in the vicinity of industrial area. *Environ. Monit. Assess.*, **73**, 263–273.
- Muntean, V. (1995-1996) Bacterial indicator of mud quality, *Contribuții Botanice*, **33**, pp. 73-76.
- Muntean, V., Crisan, R., Pasca, D., Kiss, S., Drăgan-Bularda, M. (1996), Enzymological classification of salt lakes in Romania, *Int. J. Salt Lake Res.*, **5** (1), 35-44.
- Muntean, V., Groza, G., Nicoară, A., Fărcaș, S., Mureșan, I. (2006) Enzymological study on iron mine spoils submitted to bioremediation, *Stud. Cercet., Biologie (Bistrița)*, **11**, pp. 109-116.
- Ottow, J.C.G. (1968) Evolution of iron-reducing bacteria in soil and the physiological mechanism of iron reduction in *Aerobacter aerogenes*. *Z. Allg. Mikrobiol.*, **8**, 441-443
- Pochon, J (1954) *Manuel Technique d'Analyse en Microbiologie du Soil*, La Turelle, Saint-Mande.
- Visser, S., Parkinson, D. (1992) Soil biological criteria as indicators of soil quality: soil microorganisms, *Am J Altern Agr*, **7**, 33–37.
- Wickham, G.S., Atlas, R.M., Ronald, M. (1988), Plasmid frequency fluctuations in bacterial population from chemically stressed soil communities, *Applied and Environ. Microbiol.*, **54**, 2192–2196.
- Wuertz, S., Mergeay, M. (1997), The impact of heavy metals on soil microbial communities and their activities, In: Van Elsas J.D., Trevors J.T., Wellington E.M.H. (eds), *Modern Soil Microbiology*, Marcel Dekker, New York, 607–639.
- *** (1997) Ordin nr. 756 din 3 noiembrie 1997 pentru aprobarea Reglementării privind evaluarea poluării mediului, Ministerul Apelor, Pădurilor și Protecției Mediului, București.